AD705078

FINAL REPORT

Supporting Investigation

MIPR No. Z-70099-9-92317

HAZARDS OF LNG SPILLAGE IN MARINE TRANSPORTATION

FEBRUARY 1970

Prepared for

DEPARTMENT OF TRANSPORTATION
U.S. COAST GUARD
Hazardous Materials Division
Washington, D.C.

DDC
RECEIVED
MAY 12 1970
B

Reproduced by the
CLEARINGHOUSE
for Federal Scientific & Technical
Information Springfield Va. 22151

by

U.S. DEPARTMENT OF THE INTERIOR
BUREAU OF MINES
Pittsburgh, Pennsylvania

This document has been approved for public release and sale its distribution is unlimited.

FINAL REPORT

HAZARDS OF LNG SPILLAGE IN MARINE TRANSPORTATION

February 1970

Prepared by:
D. S. Burgess
J. N. Murphy
M. G. Zabetakis

SRC Report No. S-4105

Distribution of this document is unlimited. This report has been prepared by the Department of the Interior, Bureau of Mines, for the Hazardous Materials Division, U. S. Coast Guard, under MIPR No. Z-70099-9-92317. The contents of this report reflect the views of the contractor, who is responsible for the facts and the accuracy of the data presented herein, and do not necessarily reflect the official view or policy of the Coast Guard. This report does not constitute a standard, specification or regulation.

APPROVED:

David S. Burgess

David S. Burgess (Acting)
Robert W. Van Dolah
Acting Research Director
Safety Research Center

U. S. Department of the Interior
Bureau of Mines
Pittsburgh, Pennsylvania

TABLE OF CONTENTS

		Page
FOREWORD		1
ABSTRACT		2
I	INTRODUCTION	2
II	ACKNOWLEDGEMENT	3
III	EXPERIMENTAL ARRANGEMENTS AND OBSERVATIONS	3
	A. Sources of LNG	3
	B. Small-Scale Experiments	3
	1. Heat Transfer Experiments	3
	2. Underwater Release of LN	6
	3. Foaming of LNG	6
	C. Large-Scale Experiments	6
	1. Spill Tests	6
	2. Dispersion Tests	7
	a. Gas Sampling	7
	b. Gas Sources	8
IV	EXPERIMENTAL RESULTS	8
	A. Heat Transfer	8
	1. Evaporation Rate of LNG from Water, Ice and Brine	8
	2. Evaporation Rates of Liquid Nitrogen	10
	3. Transient Temperatures under the Water Surface	10
	B. Frothing of LNG, LN_2 and Liquid Methane	11
	C. Spreading of LNG on an Extended Water Surface	11
	D. Atmospheric Dispersion	13
	1. Wind Velocity and Wind Direction Near a Water Surface	13
	2. Wind Direction as Function of Duration of Observation	13
	3. Gas Concentrations Downwind of a Steady Source	15
	4. Determination of σ_y	16
	5. Determination of σ_z	16
	6. Concentration as a Function of Distance	17
	7. Peak-to-Average Ratios	19
V	DISCUSSION	19
	A. Heat Transfer and Evaporation Rates	19
	B. Spreading of LNG on an Extended Water Surface	23
	C. Concentrations Downwind from a Natural Gas Source	24
	1. Concentrations Close to the Source	28
	2. Ratios of Peak Concentration to Average Concentration	30
	3. Cold Gas Layering	30
	D. Explosion Hazard (Without Ignition)	31
VI	CONCLUSIONS AND RECOMMENDATIONS	34

PRECEDING PAGE BLANK

TABLES

		Page
1.	Analysis of Laboratory Natural Gas, of LNG Condensed therefrom, of Liquid Methane, and of Commercially Supplied LNG	4
2.	Observed Evaporation Rates and Calculated Heat Fluxes in Spillage of Cryogens	9
3.	Thermal Diffusivity of Ice from the Data in Figure 8	14
4.	Angular Deviations, Test 10, June 22, 1969	14
5.	Observed and Calculated σ_y at 50 Feet from a Natural Gas Source	18
6.	Calculated Vertical Standard Deviation, σ_z	18
7.	Centerline Concentrations at 50 feet in LNG Dispersion	18
8.	Peak-to-Average Ratios, Test #7	20
9.	Peak-to-Average Ratios, All Stations	20
10.	Calculated Vaporization Rates in Large Spills	25
11.	Some Representative Atmospheric Conditions	27

ILLUSTRATIONS

Fig.

1. Schematic of apparatus for small-scale spillage.
2. Spills of (a) LNG and (b) liquid nitrogen at comparable times during the first 10 seconds of contact with 5 gallons of water in a 2x1x1-ft aquarium.
3. Arrangement of test site for large-scale experiments.
4. Spreading of 50-gallon spill of LNG over water.
5. Selected frames of a motion picture sequence showing the "explosion" when 70 gallons of LNG was poured onto water.
6. Vaporization of LNG on water.
7. Vaporization of LN_2 on 2-ft^2 block of ice.
8. Temperature profiles after LNG spills on water.
9. Temperature profiles after LN_2 spills on water.
10. Apparent depths of LNG, liquid methane and LN_2.
11. Pool diameter as function of time after LNG spills on water.
12. Maximum diameters and durations of LNG spills on water.
13. Wind speed and wind direction: a representative recording near a water surface.
14. Wind speed and standard deviation of direction.
15. Schematic of vapor trail and plume.
16. Representative responses of methane sensors during release of natural gas.
17. Gaussian distribution curves of natural gas concentration, test 11.
18. Cumulative frequency distribution calculated from concentration data of test 11.

Fig.

19. Vertical distribution of concentrations at 50 ft from LNG source.
20. Natural gas concentrations at 50 and 125 ft from source.
21. Peak (3 seconds) and average (10 minutes) concentrations, 50 ft from a natural gas source.
22. Heat transfer rates to liquid methane and to LN_2 from conductive warm surfaces.
23. Manson's model for periodic film boiling heat transfer.
24. Predicted vaporization rate, 1,000-gallon spill of LNG on water.
25. Concentration profile downwind from an LNG spill into a diked area (from reference 7).
26. Plume extending downwind from a spill.
27. Nomograph pertaining to concentrations near a small natural gas source.
28. Nomograph pertaining to concentrations at long distances from a natural gas source.
29. Frequency of small-scale explosions in LNG dispersion test, one lb/sec LNG poured onto water.

HAZARDS OF LNG SPILLAGE IN MARINE TRANSPORTATION

FOREWORD

This report was prepared by the Safety Research Center of the U. S. Bureau of Mines as the concluding item under MIPR Z-70099-9-92317 of December 3, 1968. Experimental work was conducted from December 1968 through June 1969. Six monthly letter reports were submitted and a briefing was performed on July 18, 1969.

The work was carried out under the cognizance of W. E. McConnaughey of the U. S. Coast Guard and was administered at Pittsburgh by R. W. Van Dolah. Participating investigators were D. Burgess, J. Murphy, M. Zabetakis, R. Mattes, H. Grainger and A. Slaypoh.

This report was submitted on September 15, 1969, and has been reviewed and approved.

PRECEDING PAGE BLANK

HAZARDS OF LNG SPILLAGE IN MARINE TRANSPORTATION

Final Report

ABSTRACT

An investigation of the hazard of spillage of liquefied natural gas (LNG) onto water is described. About 2000 gallons of LNG were consumed in various tests. The initial vaporization rate of LNG following spillage was found to be 0.037 lbs/ft^2 sec; when the spill was confined, this vaporization rate was moderated after about 20 seconds by the growth of an ice layer on the water surface; when the spill was unconfined, a coherent ice floe was not observed and the vaporization rate was essentially time-independent. The maximum diameter (in feet) of the spreading LNG pool was found to be given by 6.3 $W^{1/3}$ where W is the weight of LNG in pounds. Downwind of a natural gas source, time-averaged methane concentrations were given in good approximation by standard air pollution equations. However, peak concentrations were as much as twentyfold higher than average, adding an additional factor to the assessment of hazard. The effect of layering by the cold vaporized natural gas was similar to the effect of a temperature inversion on normal gases in the atmosphere.

Small-scale explosions were observed on pouring LNG onto a water surface. These explosions are discussed but no single explanation seems pertinent to all of the incidents observed.

I INTRODUCTION

The Bureau of Mines has made a previous study of the handling hazards of liquefied natural gas (LNG).[1/] This earlier effort was directed mainly to the ignition and combustion characteristics of the spilled liquid and was based on the assumption of aboveground storage of LNG with the possibility of spillage within a diked area.

By 1968 it was evident that some new studies were desirable because of the imminence of marine transportation of LNG into American harbors. If LNG is released onto water, as might occur in a ship collision, there are several new aspects of the safety problem which were not considered in the earlier study: first, the evaporation rate of LNG in contact with water is substantially higher than that from a dry surface; second, the LNG may be free to spread over an indefinitely large area with an accompanying magnification of its rate of evaporation; finally, the flammable cloud of natural gas/air may extend for large distances downwind because of the absence of topographic features which normally promote turbulent mixing.

1/ Burgess, D., and M. G. Zabetakis. Fire and Explosion Hazards of Liquefied Natural Gas. Bureau of Mines Report of Investigations 6099, 1962, 34 pp.

In the course of this present investigation two unforeseen phenomena were encountered. One was a frothing of the spilled LNG to cause it to occupy several times its initial volume. This was considered to be of more interest in fixed installations (larger diked volumes would be required) than in marine transportation and was not studied in detail. The other was associated with a variety of explosion phenomena which accompanied the pouring of LNG onto water. While there was never an ignition of the natural gas, there was enough energy release to cause equipment damage and to promote dispersion of the liquid within very short time intervals. A systematic study of the mechanisms of these explosions was not within the scope of this effort, however the present report contains descriptions and photographs of explosions and a recommendation for further study.

II ACKNOWLEDGEMENT

Since the scale of test operations was directly dependent on the availability of LNG, we were fortunate to have had the cooperation of LNG Services, Inc., Pittsburgh, Pa., who delivered LNG directly to our storage dewar at Bruceton in quantities up to 800 gallons.

III EXPERIMENTAL ARRANGEMENTS AND OBSERVATIONS

A. Sources of LNG

For the initial small-scale experiments, LNG was obtained by condensing pipeline natural gas with liquid nitrogen. The condensing apparatus was a closed system designed to eliminate preferential condensation of the higher boiling point constituents. Gas chromatographic analyses of the pipeline gas and the LNG condensed therefrom are shown in table 1. In several cases, pure (99.75 percent) methane was condensed in the same manner.

Samples of LNG for analysis were obtained by immersing a pipette into the LNG, after which connection was made to an evacuated sample bottle and the total contents of the pipette collected in the bottle.

For the large-scale experiments, the LNG was purchased commercially and stored in an 800-gallon dewar. An analysis of this LNG is also shown in table 1. About 2,000 gallons of LNG were consumed in the program.

B. Small-Scale Experiments

1. Heat Transfer Experiments. The small-scale experiments used to obtain heat transfer and vaporization data were conducted in a 2x1x1 foot deep aquarium (figure 1). The cryogenic liquid was contained in an open mouth dewar which was positioned in a remotely actuated dumping apparatus. The aquarium had a metal ramp just below the surface of the water which

TABLE 1. - Analysis of Laboratory Natural Gas, of LNG Condensed Therefrom, of Liquid Methane, and of Commercially Supplied LNG

	Natural Gas	Condensed LNG	Liquid Methane	Commercial LNG
Methane	92.9	94.5	99.75	94.9
Ethane	3.7	3.4	--	5.5
Propane	1.2	0.9	--	0.6
Butane	0.5	0.4	--	trace
Pentane	0.4	0.3	--	--
Butenes } Pentenes }	0.5	0.5	--	--
Hexane	--	--	--	--
Nitrogen	0.3	--	0.2	--
Carbon Dioxide	0.5	trace	--	trace

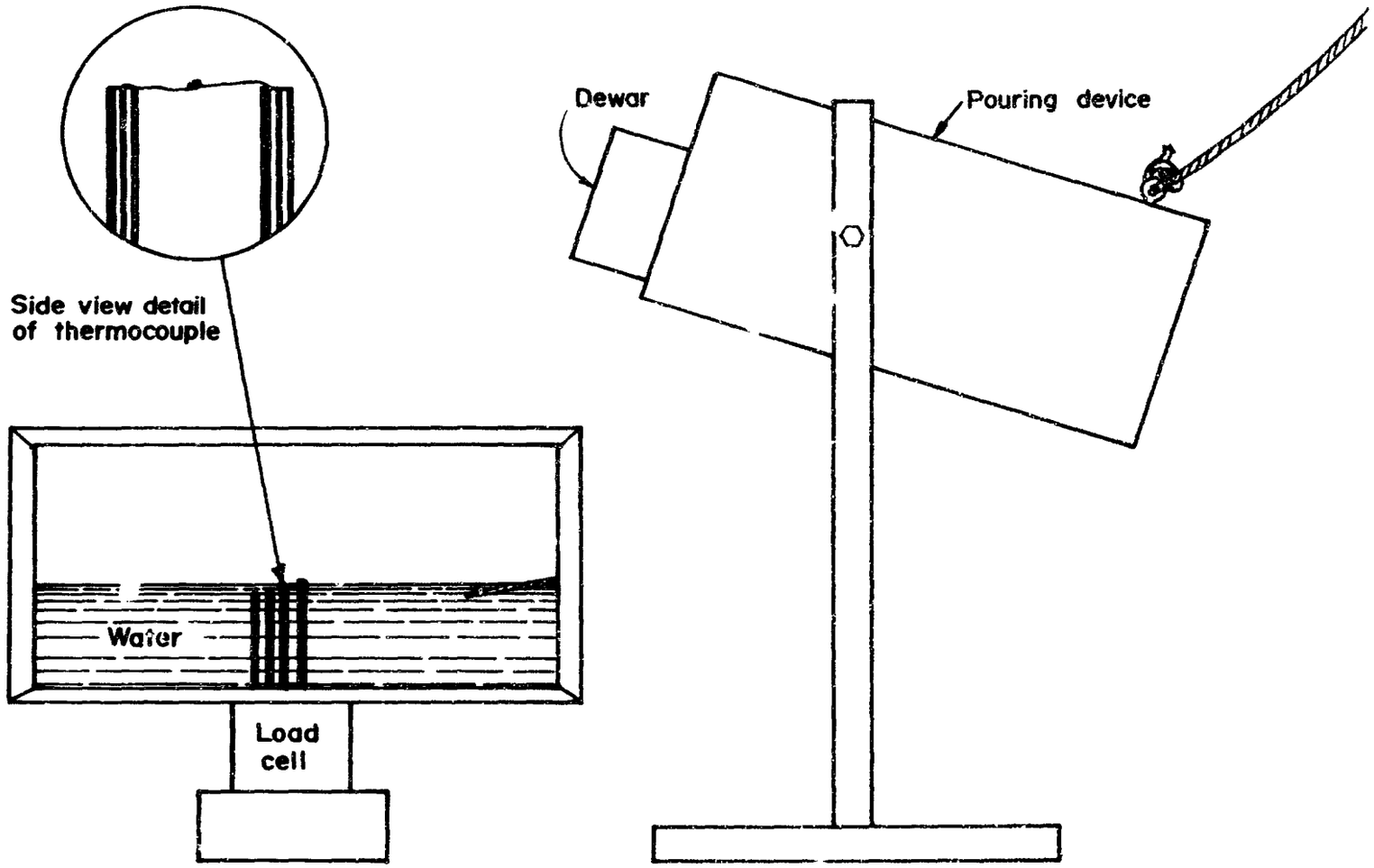

0X3-103
800

Figure 1. - Schematic of apparatus for small-scale spillage.

minimized mixing of the cryogenic liquid with the water. Motion picture and single frame sequence cameras were used on some of the experiments to observe the LNG-water interface. The aquarium was positioned on a load cell and the weight-time record was displayed on an oscillograph to obtain the vaporization rates of LNG and of liquid nitrogen (LN_2) spilled on water. The aquarium was also equipped with an array of four 4-mil diameter Chromel-Alumel thermocouples to measure temperatures near the cryogenic liquid-water interface. The initial water level was positioned at one of the four thermocouples, fixing the positions of the other three relative to the interface. The thermocouple lead wires were supported in a horizontal plane by ceramic rods (see details in figure 1) which kept them in the same nominal temperature zone as the junction to minimize heat conduction through the leads. The thermocouple signals were displayed on the same recorder used for the load cell signal.

Figure 2 illustrates the evaporation of LNG (left) and of liquid nitrogen (LN_2) from 5 gallons of water in the 2x1x1 foot aquarium. The white zone in each frame is the cloud produced by cold vapors in contact with atmospheric moisture and the underlying dark zone is the water. The LN_2 can be observed as a liquid layer while the LNG is more frothy and is not easily distinguishable in these photographs. Note particularly the violent agitation of the LN_2-H_2O interface in the right series of pictures; by contrast the LNG-H_2O interface is relatively quiet. From close inspection of these photographs we judge that a coherent ice film had formed in the nitrogen spillage test after about 10 seconds; an ice film seems to have formed in the LNG-water test at some time between 2 and 3 seconds.

Such results are probably to be expected from the relative densities of the liquids, LN_2 at 0.81 g/cm^3 being rather comparable to water while LNG at 0.42 g/cm^3 would have much greater buoyancy. The pertinent point here is that the measured heat transfer from the water to LNG should be much more reproducible than that from water to LN_2 during the first few seconds after spillage; this is borne out by experimental data.

Additional experiments were conducted in which the cryogenic liquids were poured onto flat trays of ice (12x24 inches). The ice was about 1-1/2 inches thick and had a 1-1/2-inch high ice rim around the edge; thus the cryogenic liquid contacted only ice. The ice tray was positioned on the load cell so that evaporation rates could be obtained in the same manner as those obtained with the aquarium.

Similar experiments were conducted in simulated sea water (2.9 percent NaCl in fresh water) in the aquarium. The first experiment of this series was without incident but in the second there was an explosion which destroyed the apparatus. This was the fifty-sixth in the series of

PRECEDING PAGE BLANK

small-scale spills, with no indication of any violent reaction in previous experiments. While there was no flame, there was evidence of the production of very high pressures. The mechanism for this explosion was at the time attributed to encapsulation of LNG with ice, followed by vaporization of the LNG inside the ice sphere resulting in sufficient pressure to violently rupture the ice. The incident led to several unsuccessful attempts to encapsulate LNG in ice on a larger scale.

2. Underwater Release of LNG. After the aquarium was destroyed, a series of experiments was conducted in an attempt to obtain an encapsulated pocket of LNG. A 5-gallon polyethylene container was wrapped with 3 feet of 50-grain/ft detonating cord; then the container was coated with urethane foam to minimize heat loss through the walls when the container was filled with LNG. The filled container was submerged under 15 feet of water and the detonating cord was fired to rupture the container.

3. Foaming of LNG. During the small-scale spills of LNG on ice and water it was noticed that there was considerable foaming of the LNG. In order to ascertain the extent of the foaming, several experiments were conducted within the 2-ft^3 aquarium without water. The LNG was poured into the dry aquarium and the subsequent sequence filmed with a 32-frame/sec motion picture camera.

C. Large-Scale Experiments

After completion of the small-scale experiments an additional experiment was conducted on an artificial pond at the Bruceton facility. The pond is about 200 feet across and 25 feet deep at the midpoint. A schematic of the pond is shown in figure 3; the locations of gas sensors used in later experiments are given in this same figure. Also shown is the location of the 800-gallon storage dewar and the instrument van.

1. Spill Tests. A series of experiments was conducted with LNG in quantities ranging from 1 to 125 gallons to develop a scaling law of maximum spill diameter vs spill quantity for LNG spills onto water. In spills of 10 gallons or less, the cryogenic liquid was contained in an open mouth stainless steel dewar suspended above the water on a steel cable stretched across the pond. The dewar was inverted with a lanyard from shore. For the larger spills, an open-mouth insulated bucket of 150-gallon capacity was constructed. The inner liner was polyethylene with about 4 inches of polyurethane foam between the inner wall and the outer steel jacket. The container was positioned over the pond by a crane with an 80-foot boom and remotely tipped from the shore.

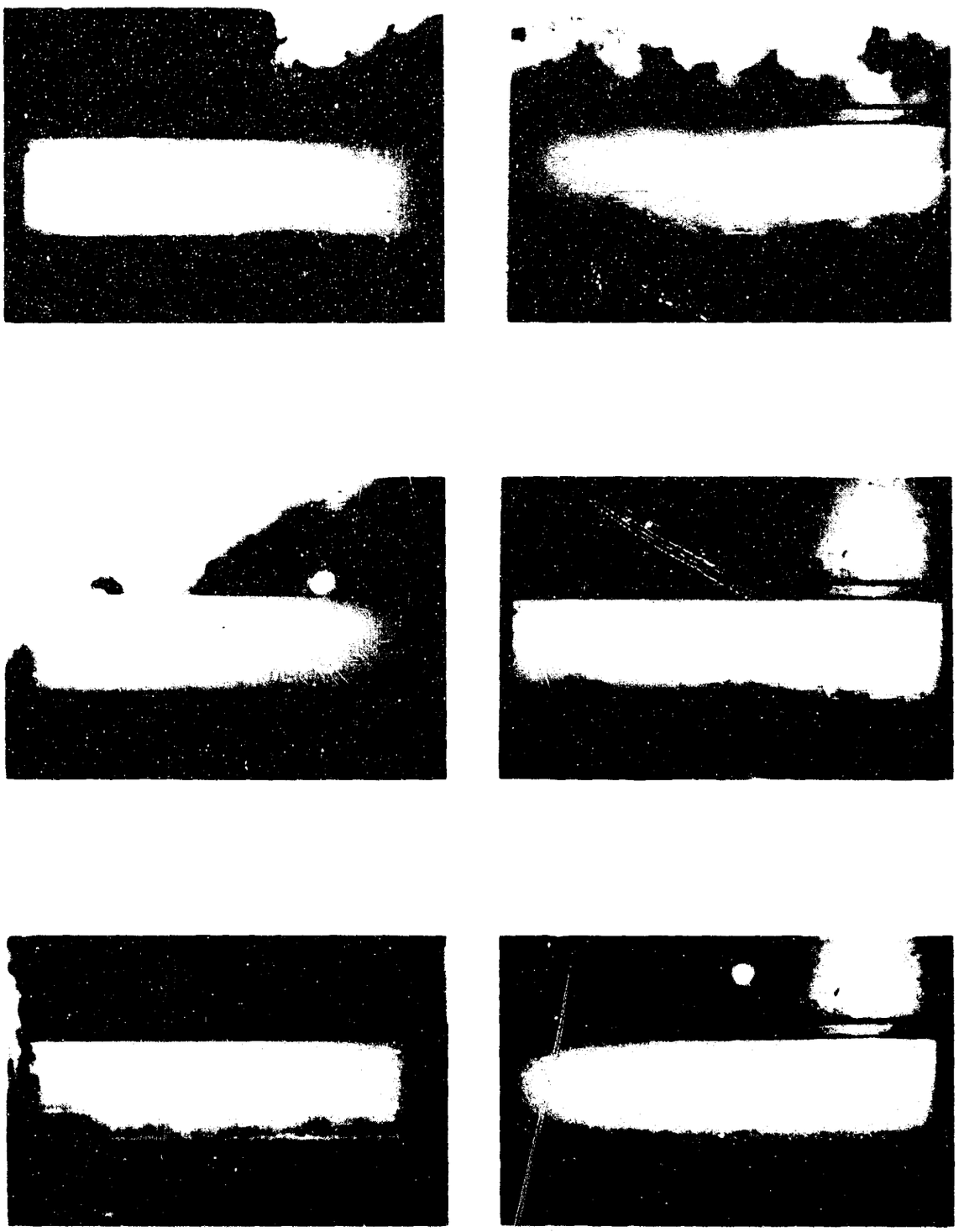

(a) (b)

Figure 2. - Spills of (a) LNG and (b) liquid nitrogen at comparable times during the first 10 seconds of contact with 5 gallons of water in a 2x1x1-ft aquarium.

PRECEDING PAGE BLANK

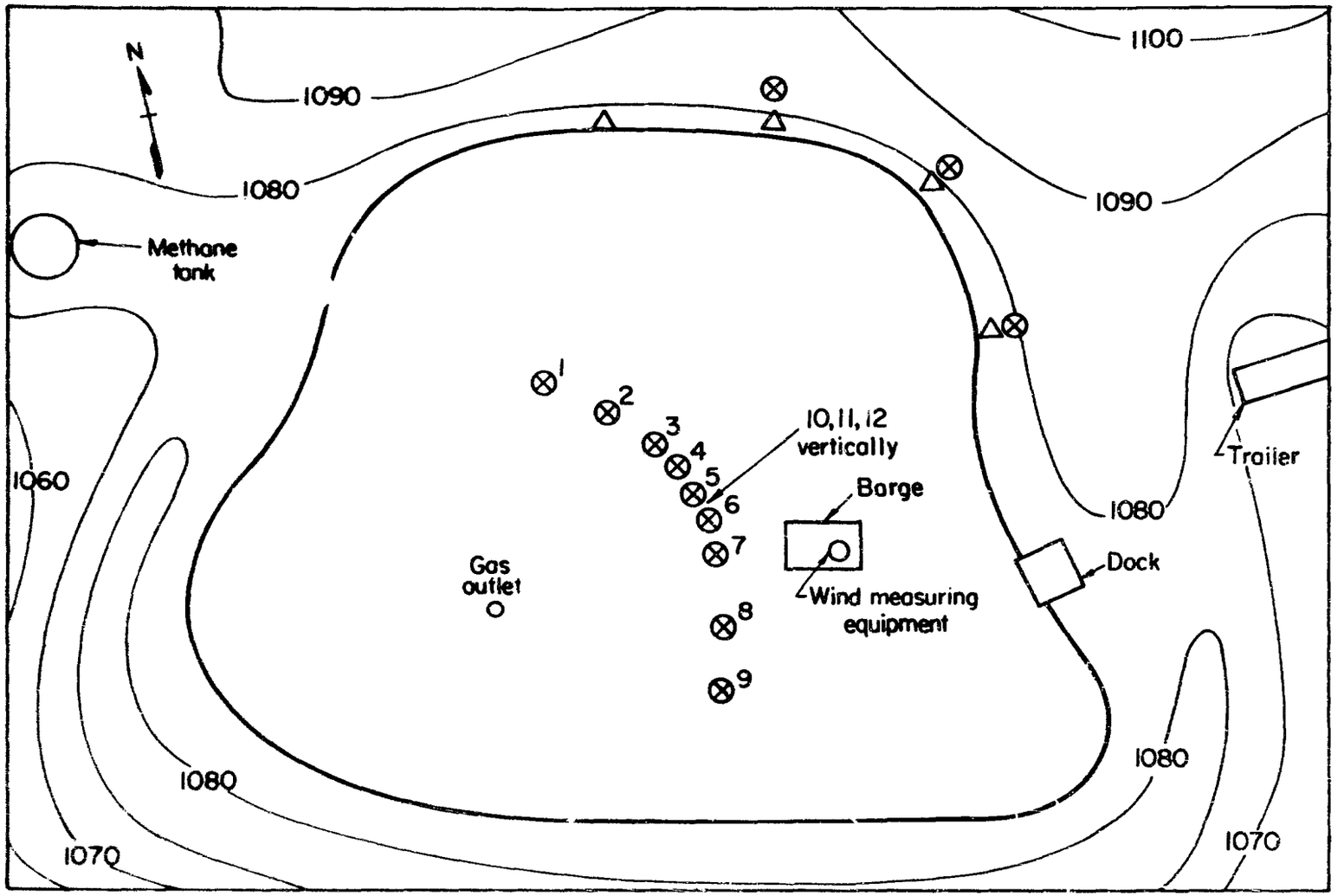

Figure 3. - Arrangement of test site for large-scale experiments.

PX3-103
809

Extensive camera coverage was provided for each of the spill tests. One or two 16-mm, 24 frame/sec color cameras were employed at ground level. In several instances, a 128-frame/sec camera was also used. Also an overhead camera was located at the tip of the crane boom to observe the spill; in small-scale tests, this was a 16-mm color movie camera; when the spill was too large for its field of view, a Hasselblad camera with a wide angle lens was installed and sequenced every two seconds with a remotely operated timer.

Figure 4 comprises a sequence of photographs from overhead after the spillage of 50 gallons LNG on the Bruceton pond. Note that the LNG spreads in a roughly circular pattern although the downwind edge is obscured by fog. At 12 seconds one observes a bare patch within the LNG pool which suggests that evaporation is nearly complete; however, there is still some residual LNG near the leading edge of the pool; it is in this region that one also observes what appear to be small ice aggregates, some of which emit jets of white fog as though LNG were entrapped in the ice. At some time after the spill, often 30-60 seconds, some of these aggregates explode with audible pops. Such disturbances were never observed with liquid nitrogen.

A different kind of explosion was obtained in one test only and is portrayed in the motion picture sequences of figure 5. The front view shows no particular activity during the first two frames (32 frames/sec); in the third frame, the white cloud is being driven outward at a velocity of at least 160 ft/sec. Most of the 70 gallons of LNG was immediately dispersed by the explosion.

2. Dispersion Tests

(a) Gas Sampling. An array of twelve Johnson-Williams Model RHE* methane sensors was located on the pond and on the shore line downwind of the gas source (figure 3) to determine how the vapor cloud from an LNG spill is dispersed; the output from each sensor was displayed on a 32-channel direct writing oscillograph located in an instrument van. The sensors were mounted on a floating rig constructed of buoys connected by angle iron. The rig formed a 102° arc of a 50-ft diameter circle with the gas source located at its center. For some experiments, all sensors were located on the rig, 9 along a horizontal and 3 in a vertical array

*Reference to trade names is made for identification only and does not imply endorsement by the Bureau of Mines.

PRECEDING PAGE BLANK

up to 15 feet above the water. In other experiments, 4 of the horizontal sensors were removed from the rig and located on the shore line at a distance of 125 feet from the gas source. Also, evacuated sample bottles with an orifice inlet requiring more than 10 minutes to bleed to atmospheric pressure were used along the shore to obtain integrated (time-averaged) gas-air samples. A wind speed and direction transducer manufactured by Sea View Electronics was located on a barge downwind from the sensors as indicated in figure 3.

(b) Gas Sources. Both pipeline natural gas and LNG were used in dispersion tests. The pipeline gas was metered by orifice (5-20 ft^3/sec) through 3-inch plastic pipe into a 22-inch diameter drum with internal diffuser plates. The drum was suspended with its open end about 18 inches above the water. In all experiments, uniform gas flow was maintained for 10 minutes.

When LNG was employed rather than warm gas, the LNG was delivered directly from the 800-gallon storage dewar through 1-1/2-inch diameter pipe, to the same drum used in the warm gas experiments. The LNG was directed up into the drum and streamed down the sides onto the water. The flow was maintained at 0.6-1.0 lbs/sec to give approximately the same mass flow as that used in the warm gas experiments.

In one instance, the LNG was directed down onto the water rather than into the drum in order to observe the effect of the initial mixing with the water.

IV EXPERIMENTAL RESULTS

A. Heat Transfer

1. Evaporation Rate of LNG from Water, Ice and Brine. During experiments comparable to those shown in figure 2, continuous (load cell) records were obtained for use in determining the weight loss of LNG by evaporation. Three sets of data are given in figure 6. Since about 3 seconds were required to pour the LNG, this early portion of the transient was not accessible to measurement. Otherwise, the weight loss vs time curves are remarkably linear through the first 20 to 40 seconds and surprisingly reproducible. Table 2 lists the average evaporation rates for six tests over the first 20 seconds as well as the maximum instantaneous loss rates which may well include some results in which spattering occurred. The comparable heat fluxes were calculated from the weight loss rates and the latent heat of vaporization of methane, 249 BTU/lb. With one exception (bracketed) the values of heat flux are within the range of values observed in the nucleate boiling of methane.[2/]

2/ Sciance, C. T., C. P. Colver, and C. M. Sliepcevich. "Pool Boiling of Methane between Atmospheric Pressure and Critical Pressure." Adv. Cryo. Eng., vol. 12, 1967, p. 395.

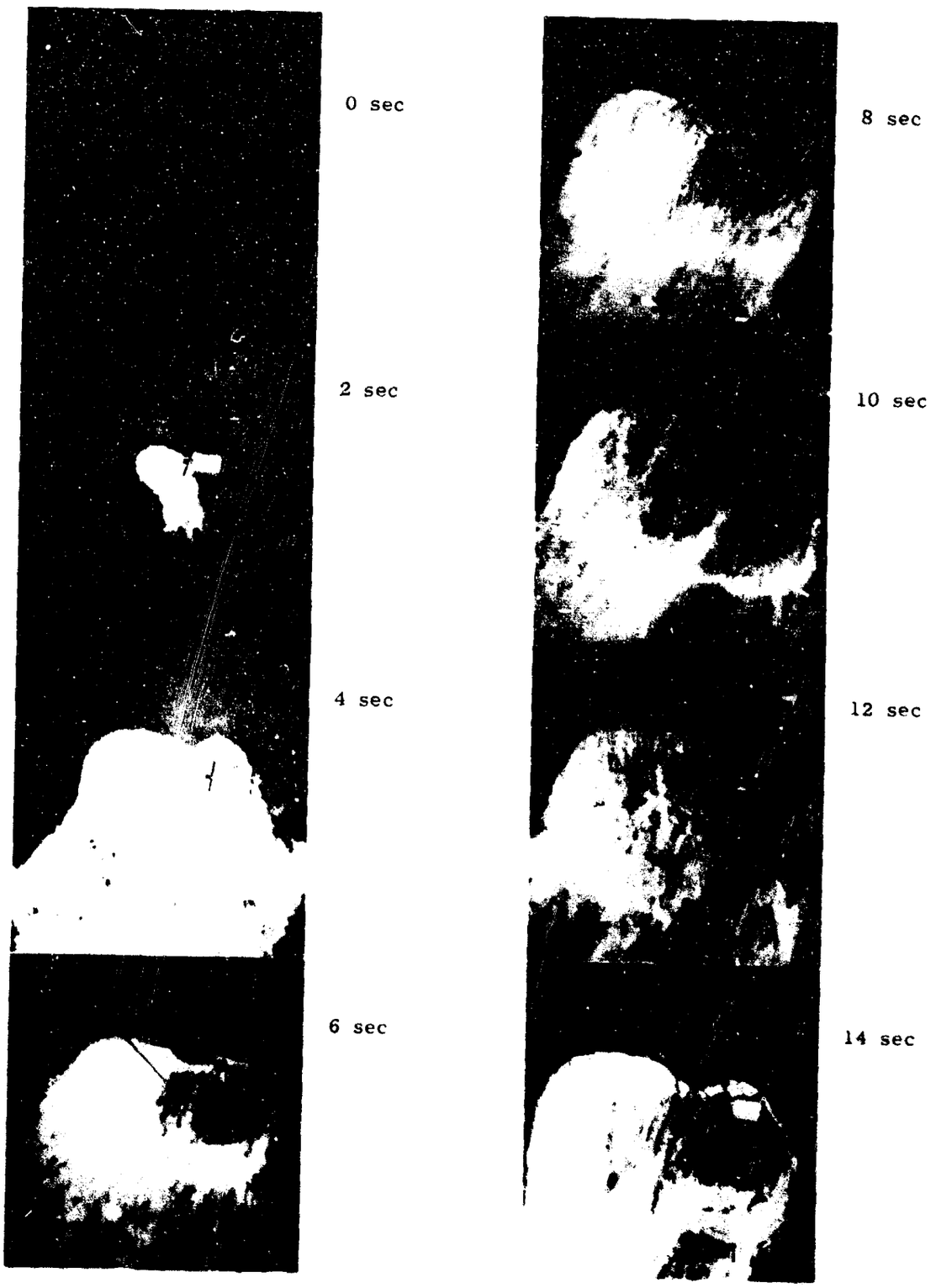

Figure 4. - Spreading of 50-gallon spill of LNG over water.

Figure 5. - Selected frames of a motion picture sequence showing the "explosion" when 70 gallons of LNG was poured onto water.

PRECEDING PAGE BLANK

PRECEDING PAGE BLANK

TABLE 2. - Observed Evaporation Rates and Calculated Heat Fluxes in Spillage of Cryogens

Test	Cryogen	Surface	Maximum Value		Average Value, 20 sec	
			Evap. Rate lbs/ft^2 sec	Heat Flux BTU/ft^2 hr	Evap. Rate lbs/ft^2 sec	Heat Flux BTU/ft^2 hr
19	LNG	Water	0.062	56,000	0.030	26,900
32	LNG	Water	.050	45,000	.039	35,000
39	LNG	Water	.047	42,200	.040	35,900
30	LNG	Ice	(.105)	(104,000)	.039	35,000
31	LNG	Ice	.068	61,000	.035	31,400
55	LNG	Brine	.052	46,700	.038	34,000
Average	LNG	All	0.064	59,000	0.037	33,000
1	Nitrogen	Water	0.070	21,600	0.035	10,800
2	Nitrogen	Water	.040	12,300	.020	6,200
6	Nitrogen	Water	--	--	.030	9,200
16	Nitrogen	Water	.032	9,900	.013	4,000
26	Nitrogen	Water	.044	13,600	.024	7,400
27	Nitrogen	Water	--	--	.032	9,900
34	Nitrogen	Water	.031	9,600	.022	6,800
21	Nitrogen	Water	.056	17,300	.032	9,900
Average	Nitrogen	Water	0.046	14,100	0.026	8,000

Table 2 includes two measurements in which LNG was poured onto ice rather than water and one in which it was poured onto 3 percent salt water. Since there were no systematic differences in the results obtained with water, ice and brine, we have simply combined the six results to obtain an average evaporation rate of 0.037 lbs LNG/ft^2 sec and the corresponding average heat flux of 33,000 BTU/ft^2 hr with standard deviations of 0.0038 lbs LNG/ft^2 sec and 3,400 BTU/ft^2 hr respectively.

2. Evaporation Rates of Liquid Nitrogen. Table 2 also shows the results of eight tests in which LN_2 was poured onto water. These data were far less reproducible than those with LNG, probably because of the highly wrinkled interface shown in figure 2. However, even with this magnification of interfacial area, the heat flux is about fourfold less with LN_2 than with LNG.

The wrinkled interface between LN_2 and the heat source was obviated by pouring LN_2 onto a cake of preformed ice; to minimize sidewall effects, pouring was done in four increments so that the maximum liquid depth was about 1/2 inch and the effective side-wall area never more than 12 percent of the horizontal surface. Results are shown in figure 7. One must look closely to observe that the evaporation rate is not time-independent. Heat flux, calculated from the slopes in figure 7a and the latent heat of vaporization of LN_2, 85.7 BTU/lb, is shown in figure 7b to decrease at first and then increase about twofold over a 2-minute period. Heat transfer during the first 20 seconds is comparable to the lowest values observed on water (table 2).

3. Transient Temperatures under the Water Surface. An array of thermocouples was positioned near the water surface to permit observation of the time-dependent heat transfer through the water to the spilled cryogenic liquid. However, the wrinkling of the cryogen-water interface spoiled the information regarding thermocouple position. It turned out then that consistent temperature transients could be obtained only at such large distances below the interface as 0.5 cm (0.2 inch). Two sets of data are shown in figure 8, representing two of the experiments included in figure 6.

From figure 8 we see there is a 15-second delay in going through the crystallization point of water at approximately 32° F, after which the temperature falls monotonically to about -200° F at 60 seconds. Fitting these data to the equation

$$T = T_o + (T_i - T_o) \operatorname{erf} (y/2\sqrt{kt}) \qquad (1)$$

one can obtain the thermal diffusivity of ice, k, at the distance y of 0.5 cm below the interface from values of temperature T, time t, and initial water temperature T_i and cryogen temperature T_o. The resultant

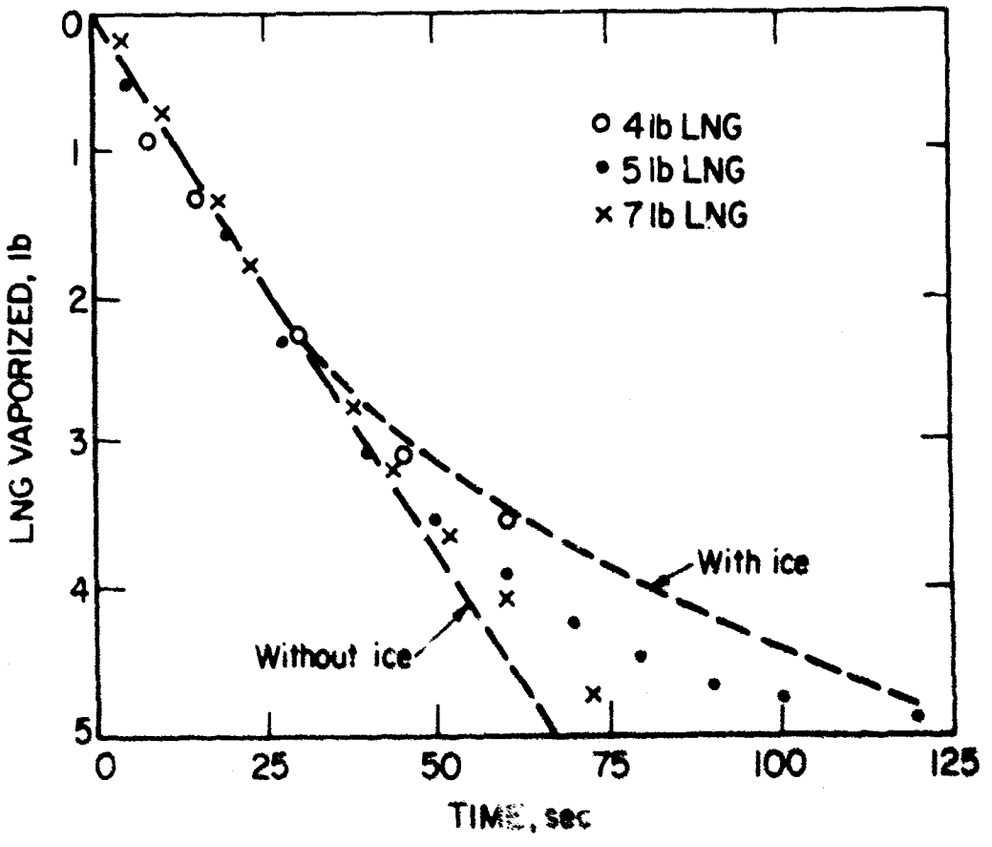

Figure 6. - Vaporization of LNG on water.

PXP-102
796

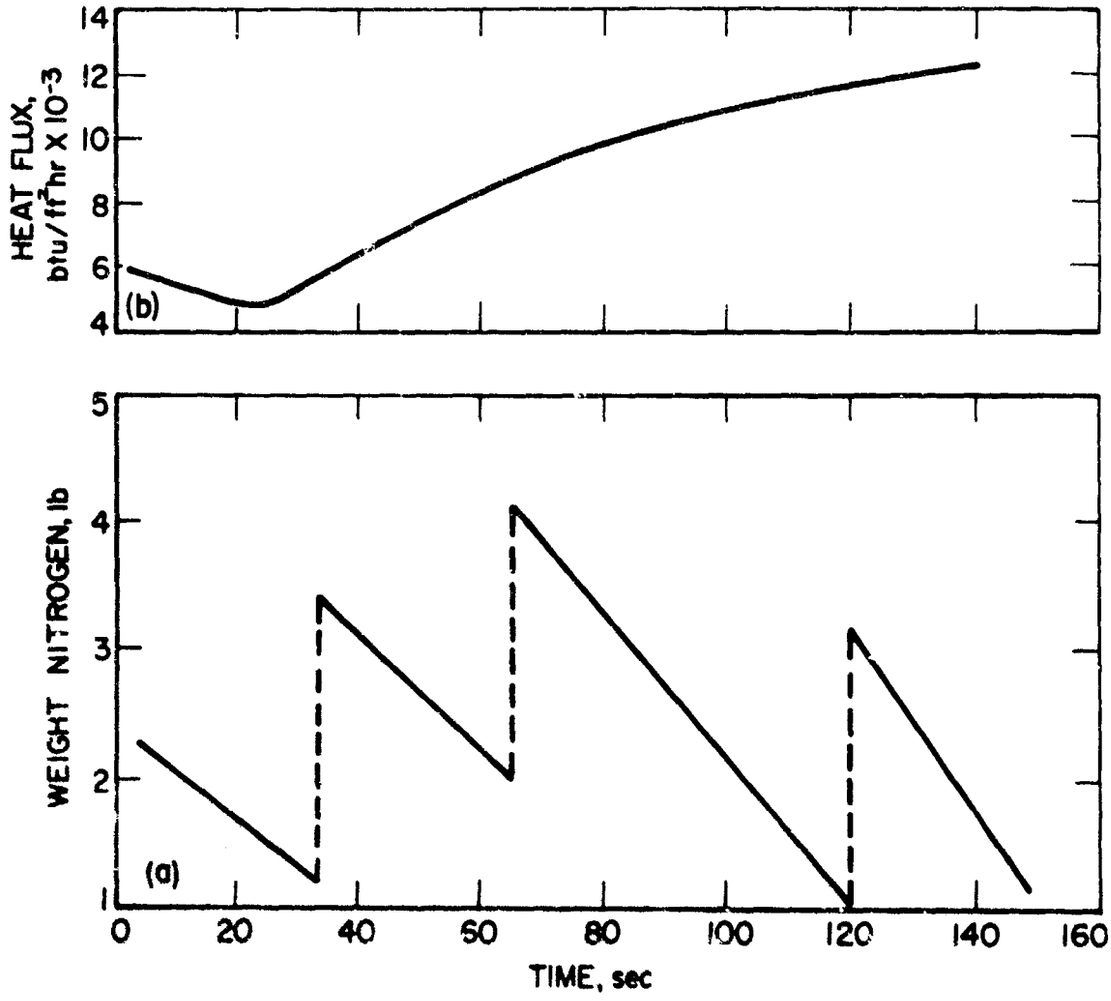

PX3-103
795

Figure 7. - Vaporization of LN_2 on 2-ft^2 block of ice (a) weight loss, (b) heat flux.

PRECEDING PAGE BLANK

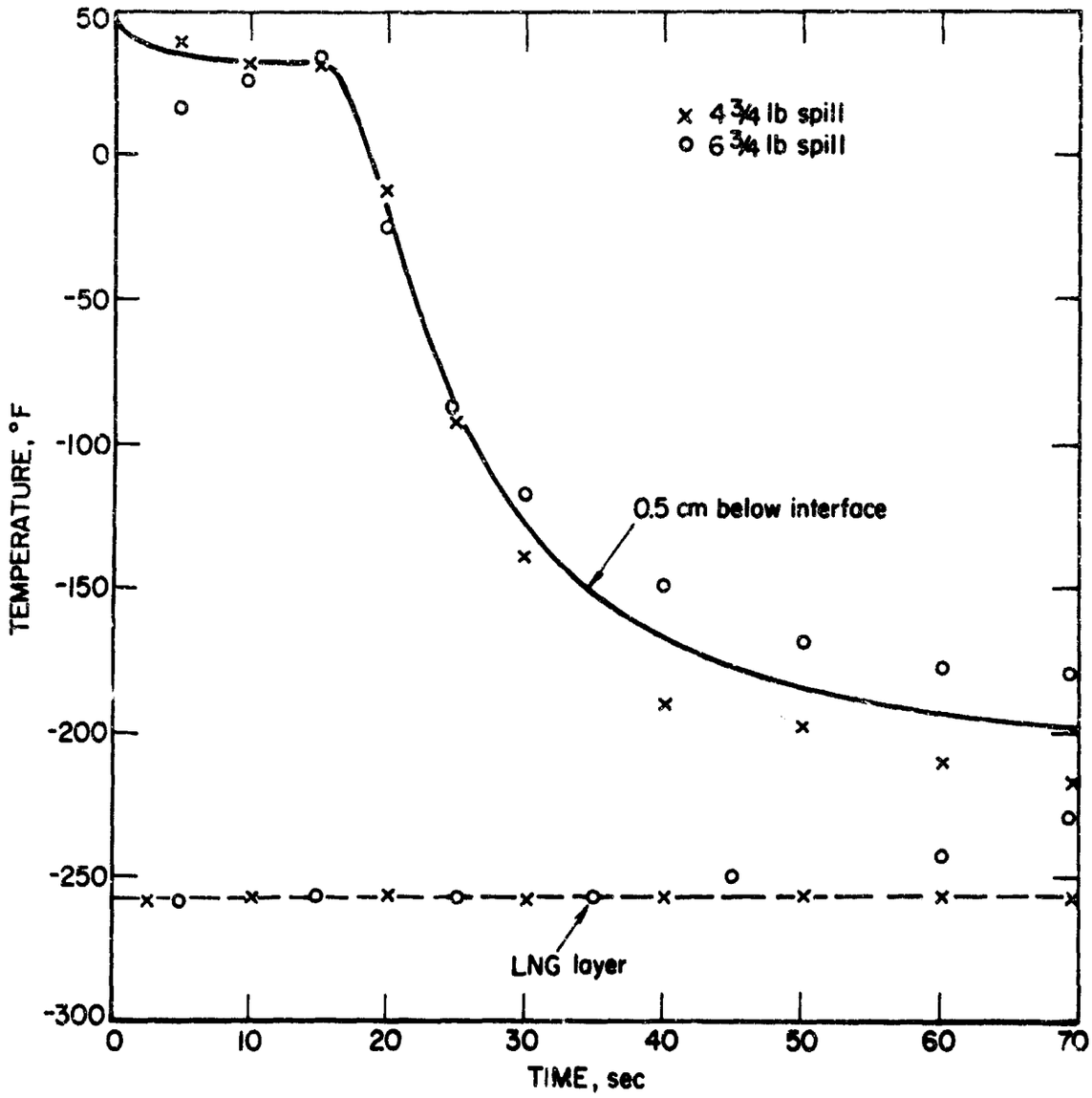

Figure 8. - Temperature profiles after LNG spills on water. PX3-103 808

PRECEDING PAGE BLANK

figures for k are given in table 3. Since k is expected to increase from 0.01 cm^2/sec at the freezing point of water to about 0.03 cm^2/sec at LNG temperature, the tabulated values (second column) are not too satisfactory. However by subtracting 20 seconds from each time interval, one obtains a reasonably constant "thermal diffusivity", k', which can be used in an empirical equation for heat conduction through ice. Finally, by subtracting 14 seconds from each time interval one obtains a "thermal diffusivity", k", which more closely resembles anticipated values. Note that this time interval of 14 seconds is approximately the delay in freezing the water in the 0.5 cm space between the thermocouple and the LNG interface.

Similar experiments were carried out with LN_2 poured onto water and the difference in curve shape is easily recognized. The points designated by crosses in figure 9 were obtained with a thermocouple located precisely at the water surface before the LN_2 was poured. Not even this thermocouple shows the rapid cooling that was observed with LNG in the 15-60 second interval. Also, there is evidence of a minimum cooling rate at about 90 seconds followed by a very rapid increase in the cooling rate and a drop toward cryogen temperature at about 120 seconds.

B. Frothing of LNG, LN_2 and Liquid Methane

The 2x1x1 ft aquarium used in the above experiments was used here but without the water. An eight liter dewar of cryogenic liquid was emptied into the aquarium and the depth of the frothing liquid was observed from motion pictures. Figure 10 shows that LN_2 occupies very little more than the nominal depth of 1.7 inches. However, LNG foams up to about a 6-inch depth during the first 10 seconds and then subsides in about half a minute. Nearly pure methane, obtained by total condensation from a cylinder, also foams but the bubbles quickly break and nominal depth is attained in less than 10 seconds.

C. Spreading of LNG on an Extended Water Surface

All spill tests on the Bruceton pond were monitored with motion picture cameras. In addition, photographs were taken at 2-second intervals from directly over the spill area. From one viewpoint or the other, it was possible to obse[illegible]ast the upwind half of each spreading LNG pool without obstruction by fog. Except in one test, the insulated LNG container was suspended close to water level and emptied by tipping so as to give as little splashing as possible.

Most of the LNG spread data appear in figure 11. In each of four small spills (3-1/2 to 6-1/2 pounds LNG), the LNG layer grew rapidly to a 6 to 8 foot diameter and then slowly to a final diameter of 9 to 10 feet. From close inspection of the motion pictures, it seemed that the

PRECEDING PAGE BLANK

first bare patch of water appeared within the spread zone at about the end of the rapid spreading rate (see arrows in figure 11). With two spills of 22 and 32 pounds LNG, a bare patch first appeared at about 10 seconds when the spill diameter was 22 to 24 feet. With 100 gallons (380 lbs) LNG, a bare patch was thought to be visible at 16 seconds when the diameter was 41 feet. A second spill of about this size (70 gallons) led to the explosion shown in figure 5. In a subsequent test, 125 gallons LNG was poured into water from a 6-foot elevation; the LNG layer attained a diameter of 40 feet in 18 seconds and eventually expanded to 44 feet.

From the results shown in figure 11, it appears that the diameter, d, increases at a nearly constant rate of 2.5 ft/sec until most of the liquid has evaporated. That is, if t is the elapsed time in seconds, then

$$d\ (ft) = 2.5\ t\ . \qquad (2)$$

Therefore the LNG area, A, is given by

$$A\ (ft^2) = \frac{\pi}{4}\ (2.5\ t)^2 = 4.9\ t^2 \qquad (3)$$

and the total rate of evaporation, $\frac{dW}{dt}$, is given by

$$\frac{dW}{dt}\ (lbs/sec) = 0.037A \qquad (4)$$

$$= 0.18\ t^2\ .$$

Integrating between zero time and τ, when the bare patch first appears

$$W_o\ (lbs) = \int_o^{\tau} 0.18\ t^2\ dt \qquad (5)$$

$$= .063\ \tau^3\ .$$

Or the time to nearly complete evaporation varies with the cube root of the initial LNG weight, W_o. That is,

$$\tau = 2.5\ W_o^{1/3}\ . \qquad (6)$$

Equation (6) gives the lower straight line on the log-log plot of figure 12. On combining (2) and (6)

$$d_{max} = 2.5\ (2.5\ W_o^{1/3}) = 6.3\ W_o^{1/3}\ . \qquad (7)$$

This gives the upper line of figure 12. The observed value of maximum diameter and time to appearance of a bare spot are plotted in this same figure.

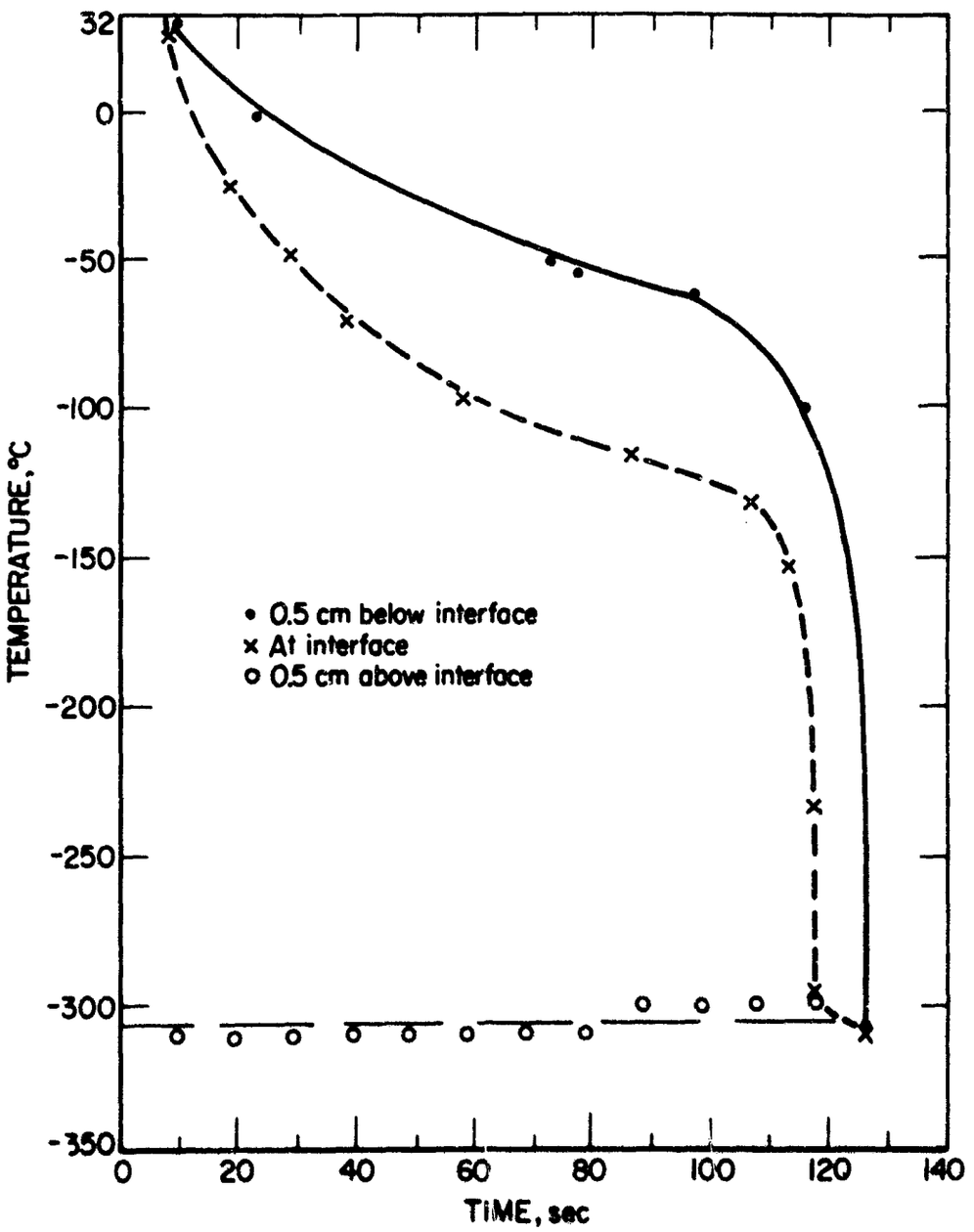

Figure 9. - Temperature profiles after LN_2 spills on water.

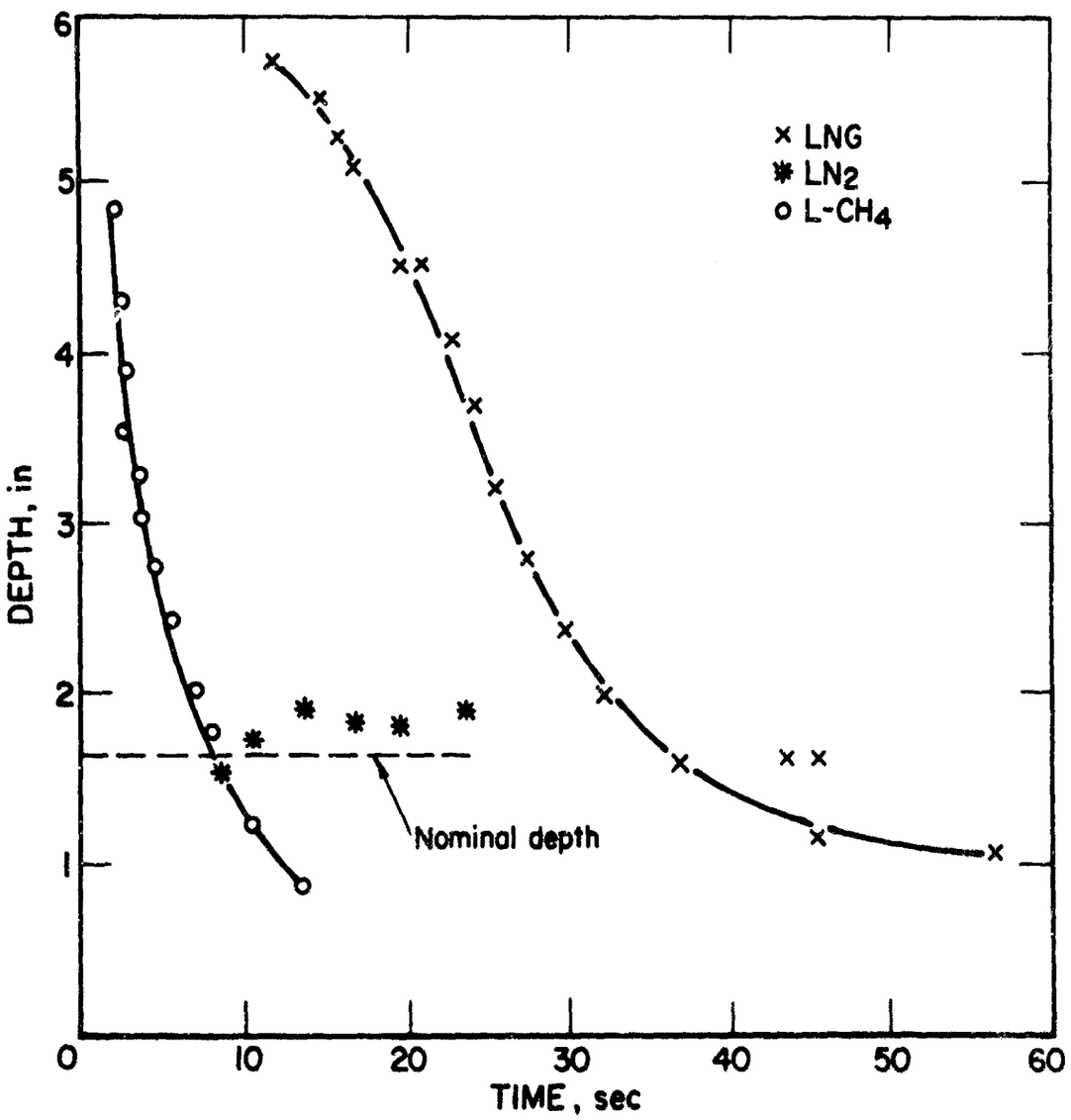

Figure 10. - Apparent depths of LNG, liquid methane and LN_2. Eight liters poured into 2x1x1-ft acquarium. PX3-103 806

PRECEDING PAGE BLANK

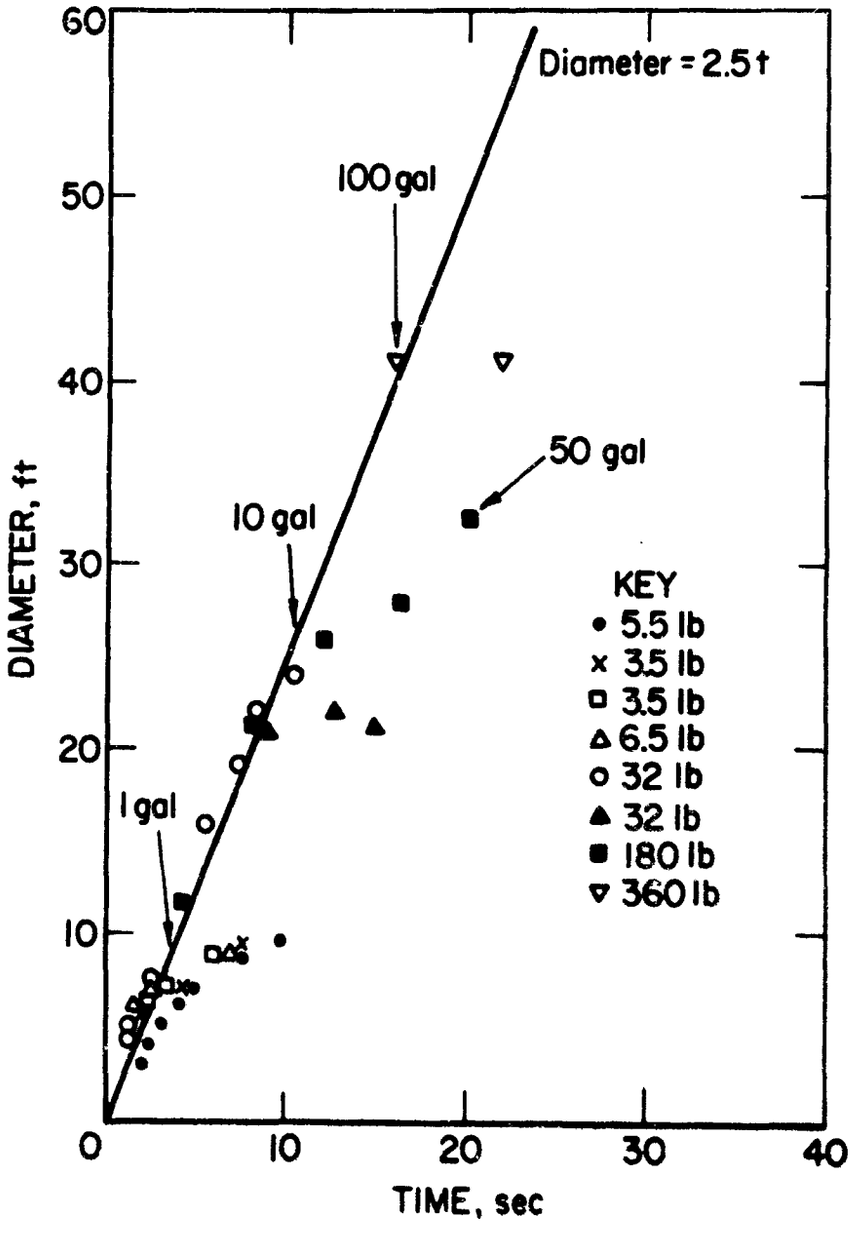

PX3-103
805

Figure 11. - Pool diameter as function of time after LNG spills on water.

PRECEDING PAGE BLANK

PRECEDING PAGE BLANK

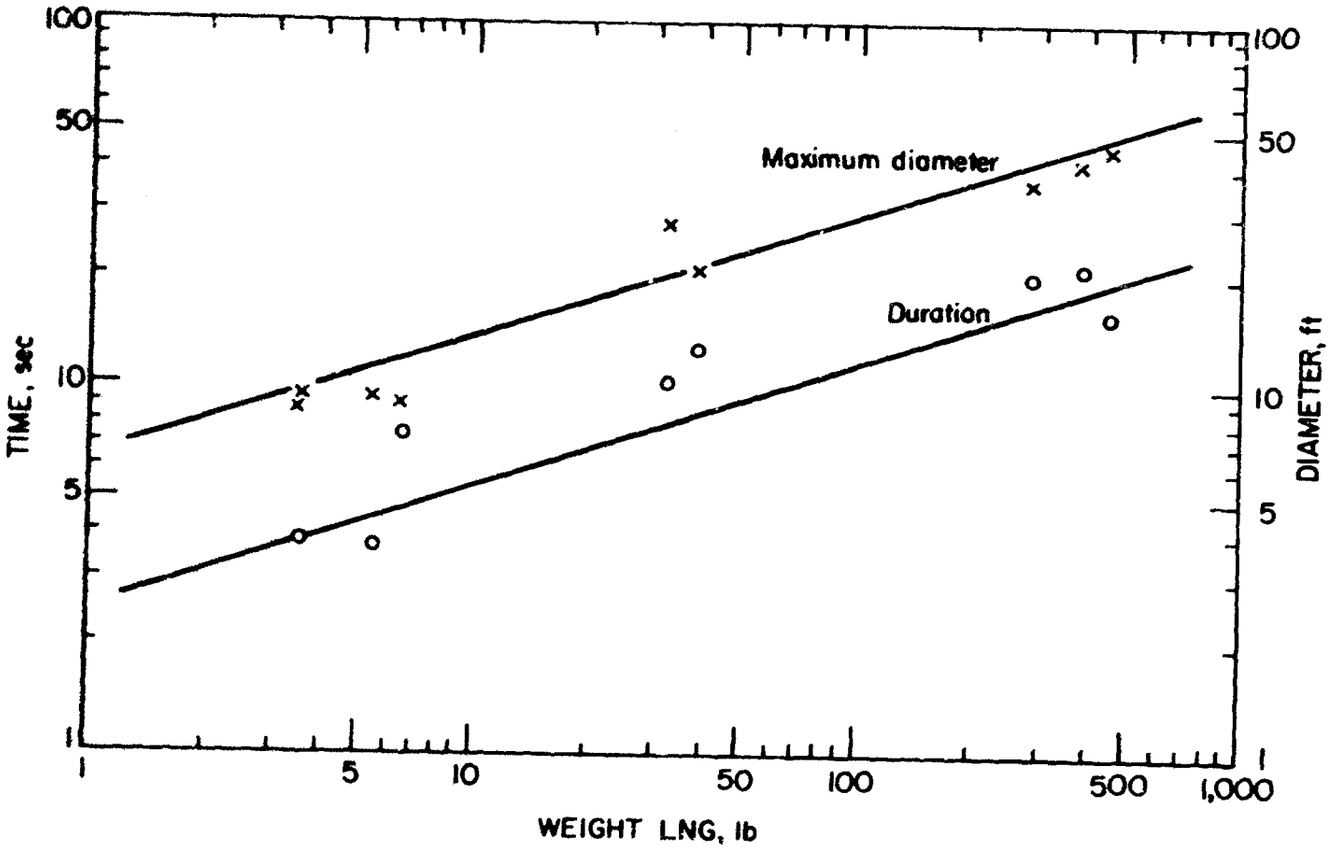

PX3-103
797

Figure 12. - Maximum diameters and durations of LNG spills on water.

D. Atmospheric Dispersion

1. Wind Velocity and Wind Direction Near a Water Surface. A short section of record from the Sea View Electronics transducer is reproduced in figure 13. The variation of wind speed (lower record) from about 2 to 9 mph and the fluctuation of wind direction within a 90° angle is typical of the B2 meteorological condition which predominated from 10 a.m. to 4 p.m. during June 1969. Wind speed and direction were normally read at 5-second intervals over periods of 10 minutes; these sets of 120 readings provided average wind speed, U, an average wind direction, $\bar{\theta}$, and the standard deviation of wind direction, σ_θ.

Since wind velocity is known to vary with height above ground level, the transducer was positioned at heights of 6, 4, 2-1/2 and 1-1/2 feet above the water surface and a large number of values of U and σ_θ were accumulated for comparison. Any systematic differences at these four heights were obscured by the general randomness of data. For this reason, during the natural gas dispersion tests, the transducer was mounted 2-1/2 feet above the water. Values of σ_θ are plotted against U on a logarithmic scale in figure 14. The local data (crosses) may be compared with a straight line which was developed from 15 years of observation at Brookhaven National Laboratory[3/] and which represents B_2, B_1, and C conditions 100 meters (325 feet) above ground level. With so little difference in results found at elevations of 2-1/2 and 325 feet, it is understandable that no trends could be identified between 1-1/2 and 6 feet.

At a given wind speed, σ_θ is consistently higher near ground level than at 325 feet; thus, if one uses standard micrometeorological data to estimate the atmospheric dispersion of a gas from a ground level source, one generally underestimates the plume width and overestimates plume concentrations; this is the desirable conservative side on which to err.

2. Wind Direction as Function of Duration of Observation. Returning to the record of figure 13, one observes that there is very little change of wind direction between 0 and 3 seconds. Therefore σ_θ is a very small angle if calculated over this short time interval. But after about 12 seconds there is a large-scale shift in wind direction which affects the average direction, $\bar{\theta}$, and therefore has a large effect on σ_θ. One finds typically that σ_θ increases toward a constant value as the period of observation is increased to about 10 minutes. The data given in table 4 pertain specifically to the record shown in figure 13.

3/ Singer, I. A., and M. E. Smith. "Atmospheric Dispersion at Brookhaven National Laboratory." Air and Water Pollution International Journal, vol. 10, 1966, pp. 125-135.

PRECEDING PAGE BLANK

TABLE 3. - Thermal Diffusivity of Ice from the Data in Figure 8

Time, sec	k cm^2/sec	k' cm^2/sec	k'' cm^2/sec
5	0.0076		
10	.0038		
15	.0026		
20	.0042		0.014
25	.0087	0.043	.020
30	.0137	.041	.026
40	.0215	.043	.033
50	.0258	.043	.036
60	.0312	.048	.042
70	.0309	.043	.039

k - t is chronological time
k' - t is chronological time minus 20 seconds
k'' - t is chronological time minus 14 seconds

TABLE 4. - Angular Deviations, Test 10, June 22, 1969

Duration of Measurement, sec	Points, No.	Average Direction, $\bar{\theta}$, °	Standard Deviation, σ_θ, °
3	7	32.0	4.28
10	21	40.1	9.44
20	21	28.6	20.03
45	18	23.1	22.51
600	114	40.9	23.45

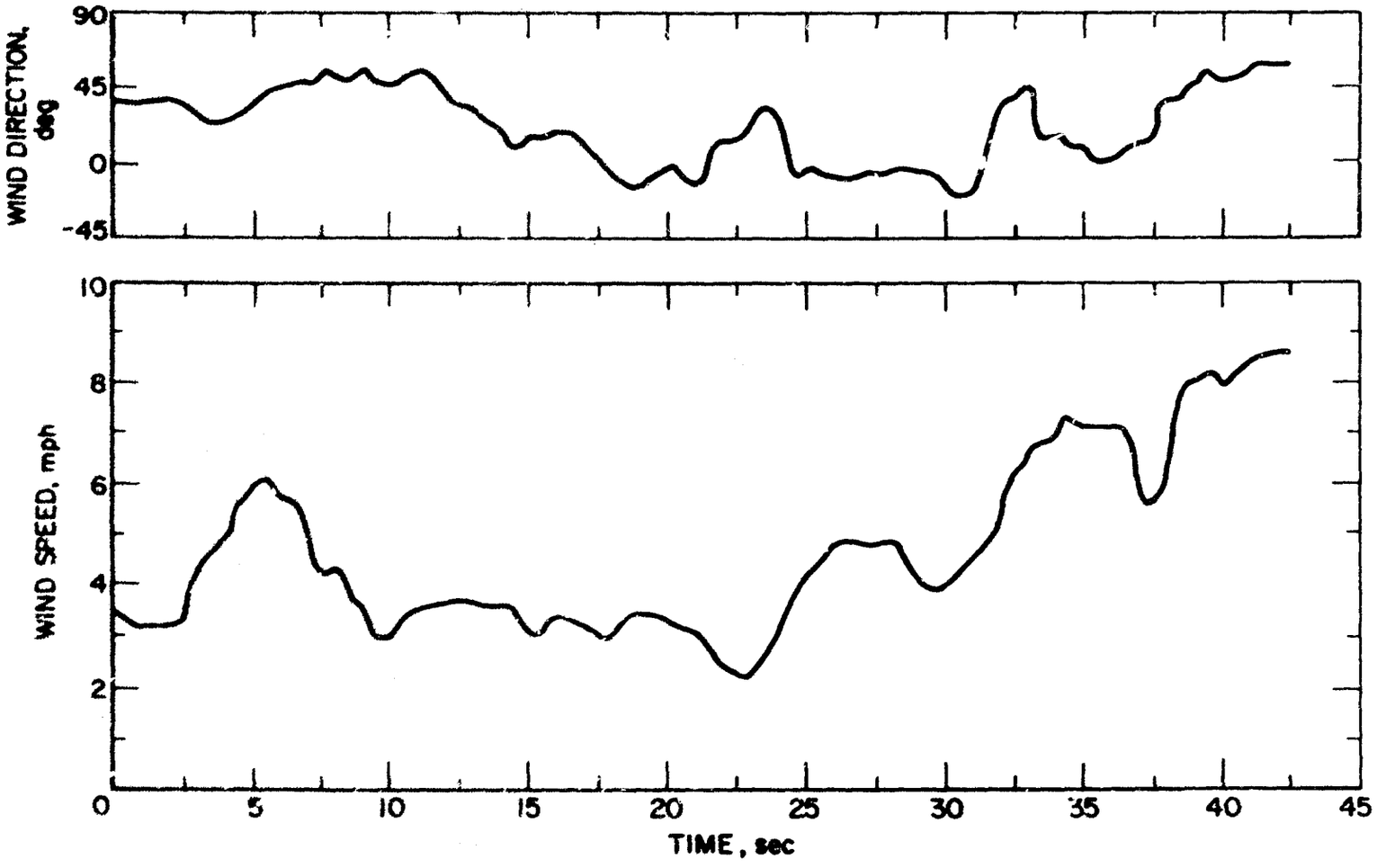

Figure 13. - Wind speed and wind direction: a representative recording near a water surface.

PK3-103
803

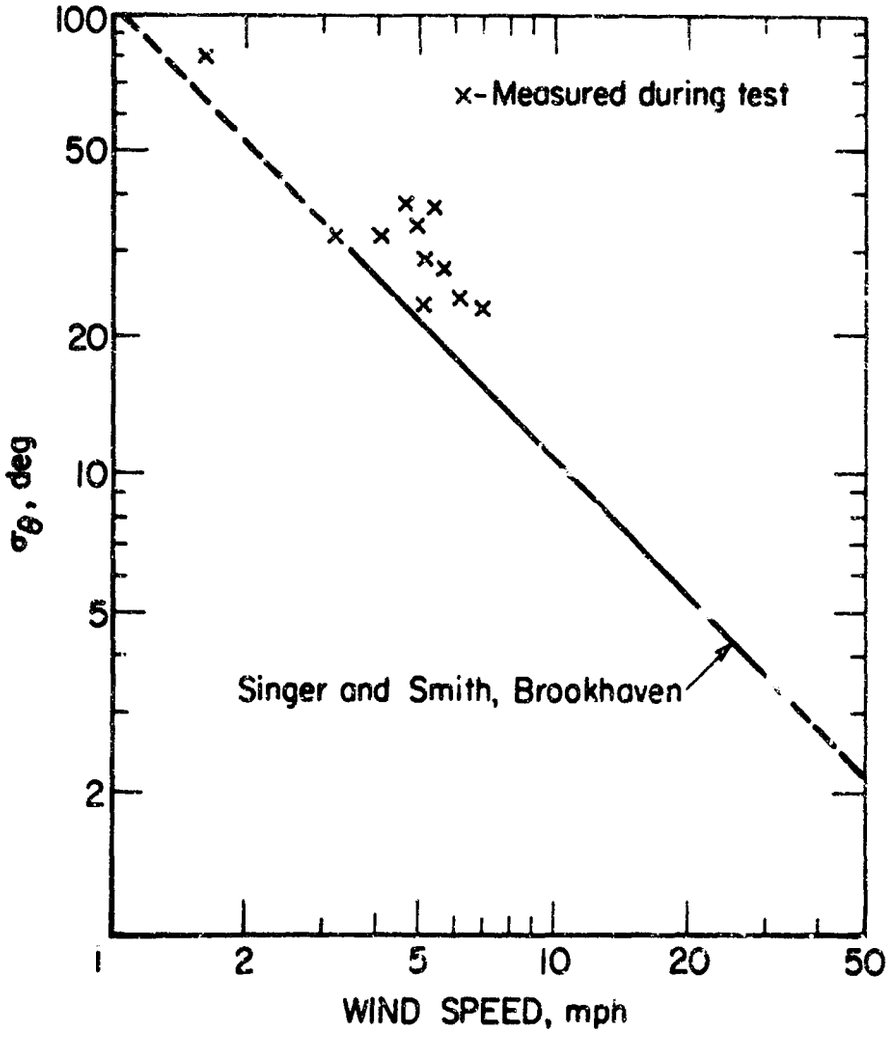

PX3-103
804

Figure 14. - Wind speed and standard deviation of direction.

PRECEDING PAGE BLANK

Figure 15 is intended to aid the visualization of terms used in the following sections. Suppose that LNG vapor is dispersed at point 0. During a 3-second interval in which the average wind direction is OX, the maximum gas concentration will be found 68 percent of the time within the small angle AOA'. This distribution of concentration is called a "vapor trail" and the maximum concentration therein is called a "peak" (we have used a 3-second time interval in this illustration because this conforms to the 95 percent response time of our methane monitors). A normal (Gaussian) distribution of concentration within a vapor trail is illustrated in figure 15 as a dashed curve; the rms displacement of concentration, σ_y, is a convenient measure of the trail's half-width and is obviously given by $\sigma_y = (OX) \tan \sigma_\theta = (x) \tan \sigma_\theta$.

Now if one considers a 10-minute interval, since the vapor trail has fluctuated through wide changes of direction in these 10 minutes, one can speak only of average concentrations. Average concentration will still follow a Gaussian distribution (solid curve) in which σ_y is still given by OX tan σ_θ but the σ_θ is the larger value associated with the 10 minute-interval (table 4). Also the time-averaged concentrations near the centerline will be much lower, as shown in figure 15. The distribution of concentrations over this long time interval is called a "plume".

3. Gas Concentrations Downwind of a Steady Source. Figure 16 shows the responses of 11 methane sensors over an interval of about one minute. The sensors labelled 1-9 were positioned in an arc of 50-foot radius with a (warm) natural gas source at the center of curvature. The sensors at the ends of the arc, numbers 1 and 9, show no response during this minute, while the sensors near the center of the array show the greatest peak concentrations (about one percent in this case) and the highest frequency of response. Sensors 10-12 measure the methane concentration at three heights near the centerline of average downwind flow.

The number of pulses observed near the centerline of flow per minute were counted and found to correspond closely to the number of times that the wind had shifted per minute through its average direction (compare figure 13). Each was shown to follow a Poisson distribution and is therefore a proper random variable.

When the warm natural gas from the pipeline was replaced with the same mass flow of LNG to give a cold dense vapor, higher concentration peaks were observed because the vertical dispersion of the heavy vapor was suppressed.

PRECEDING PAGE BLANK

4. Determination of σ_y. Figure 17 shows the average concentrations (10-minute interval) at 50 ft distances from a 20 ft^3/sec source of warm natural gas. A single stray point rather confuses the picture in this graph so that one is unsure of either the maximum concentration or the centerline of flow. However when the same data are used in a cumulative frequency distribution as shown in figure 18, a fairly good straight line results on probability paper. One standard deviation, σ_y, is included between the 15.9 and 50 percent cumulative percentage points. The value obtained, 24.5 feet, was then used to construct the Gaussian curve of figure 17. The lower curve in figure 17 was constructed on the assumption that the inverse square law is valid, that is, that σ_y would increase directly with distance between 50 and 125 feet and that all concentrations would correspondingly decrease by the ratio $(50/125)^2$.

A number of σ_y values are collected in table 5 for comparison with values predicted (fifth column) for short distances by

$$\sigma_y = x \tan \sigma_\theta \ .$$

The final column of the table gives values of σ_y as calculated from the Singer and Smith line in figure 14. The equation of this straight line is

$$\sigma_\theta = \frac{110}{\bar{U}} \qquad (8)$$

with $\bar{U}$ in mph and σ_θ in degrees. Converting to units of feet per second and radians, this becomes

$$\sigma_\theta = \frac{2.86}{\bar{U}} \qquad (9)$$

Using the approximation

$$\tan \sigma_\theta \sim \sigma_\theta \ , \qquad (10)$$

one derives

$$\sigma_y = x \tan \sigma_\theta = x \left(\frac{2.86}{\bar{U}}\right) \ . \qquad (11)$$

5. Determination of σ_z. Since it is obviously more difficult to measure the distribution of gas concentration vertically than horizontally, it is customary to invoke the expression

$$\chi_{CL} = \frac{100\ Q}{\pi \sigma_y \sigma_z \bar{U}} \qquad (12)$$

wherein Q is the flow of vapor, ft^3/sec, χ_{CL} is a measured concentration at the centerline of flow, volume percent, and $\bar{U}$ is the average wind speed,

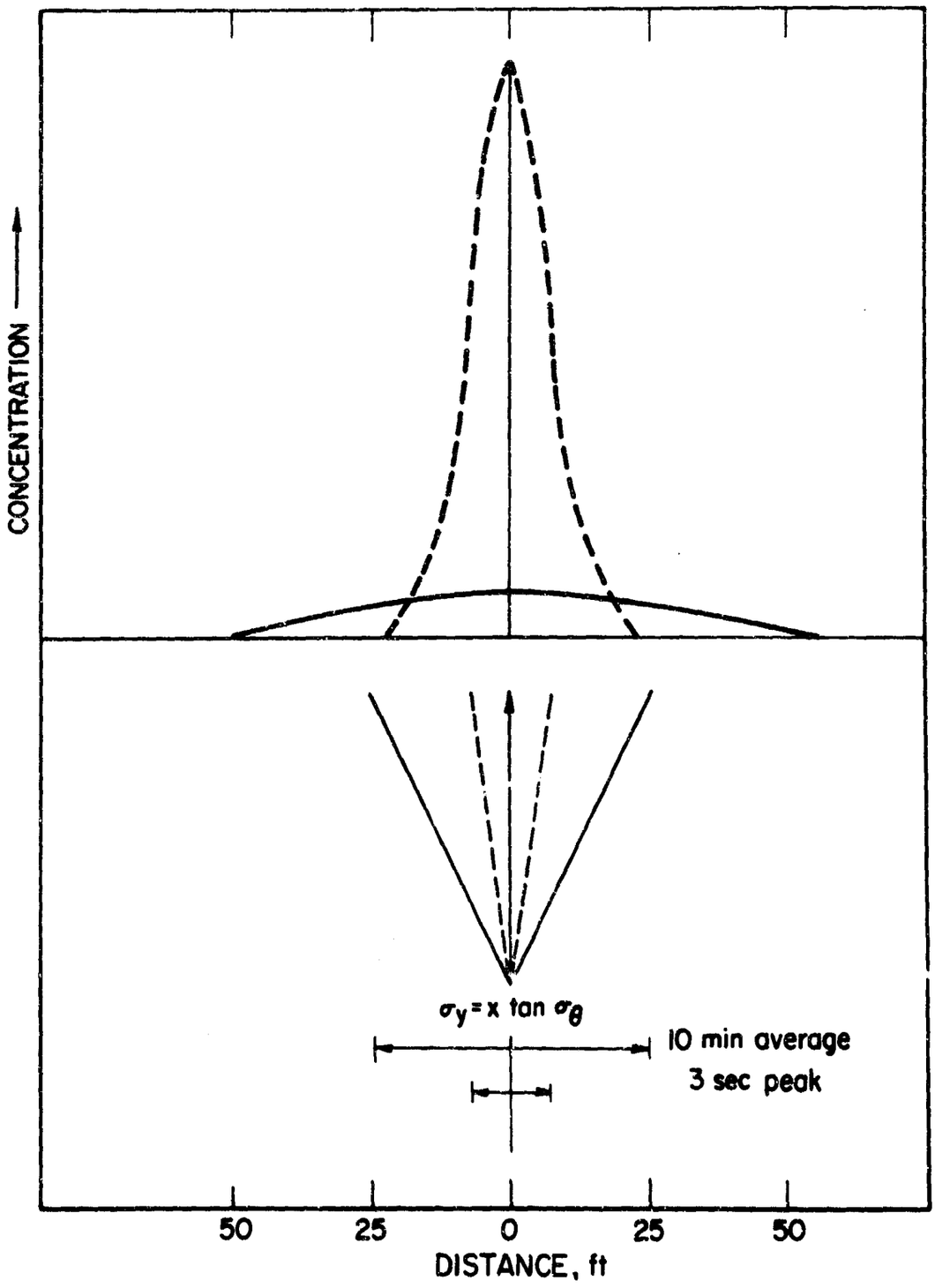

Figure 15. - Schematic of vapor trail and plume.

PX3-103
802

PRECEDING PAGE BLANK

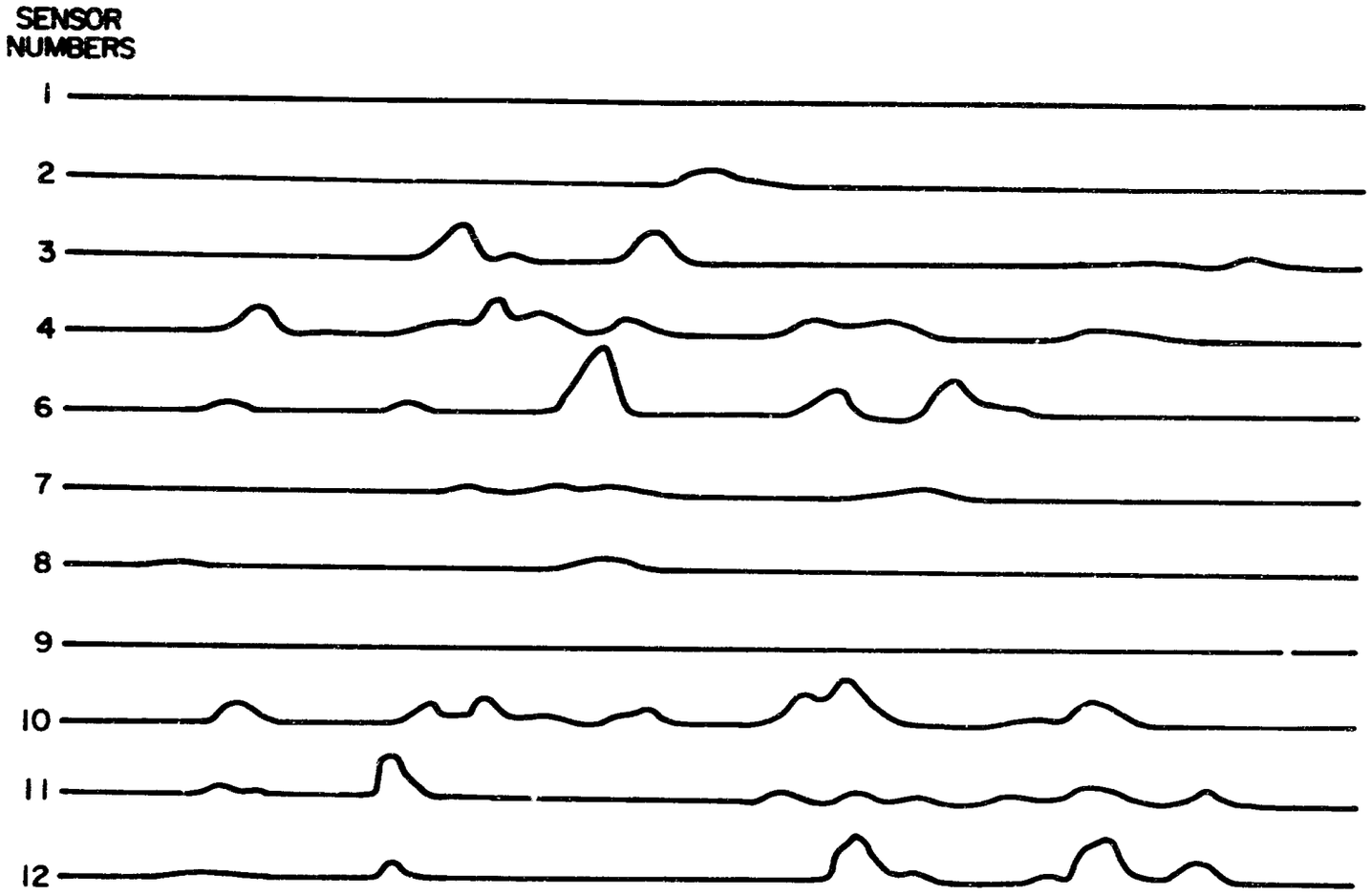

PRECEDING PAGE BLANK

Figure 16. - Representative responses of methane sensors during release of natural gas.

PX3-103
816

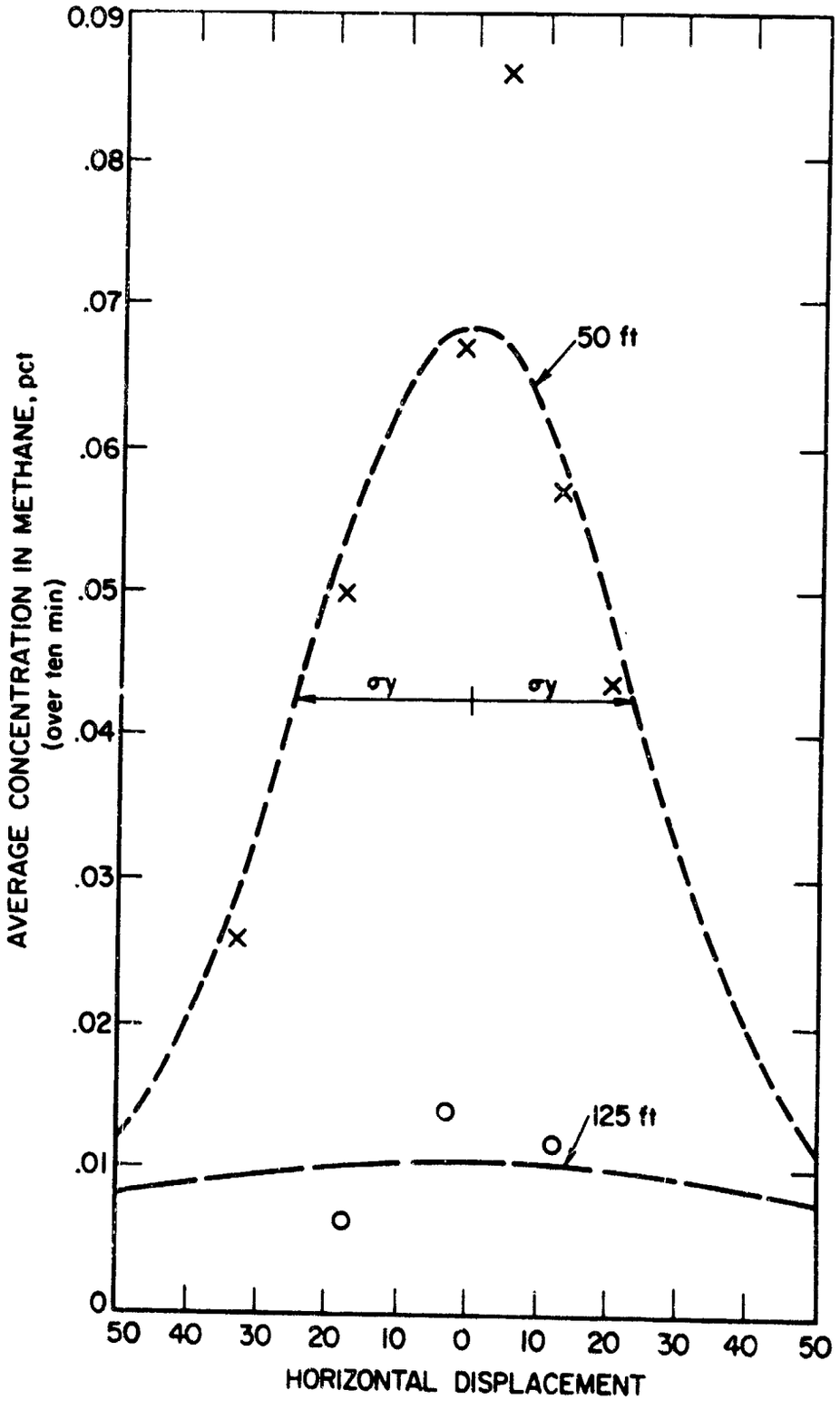

PRECEDING PAGE BLANK

PX3-103
817

Figure 17. - Gaussian distribution curves of natural gas concentration, test 11.

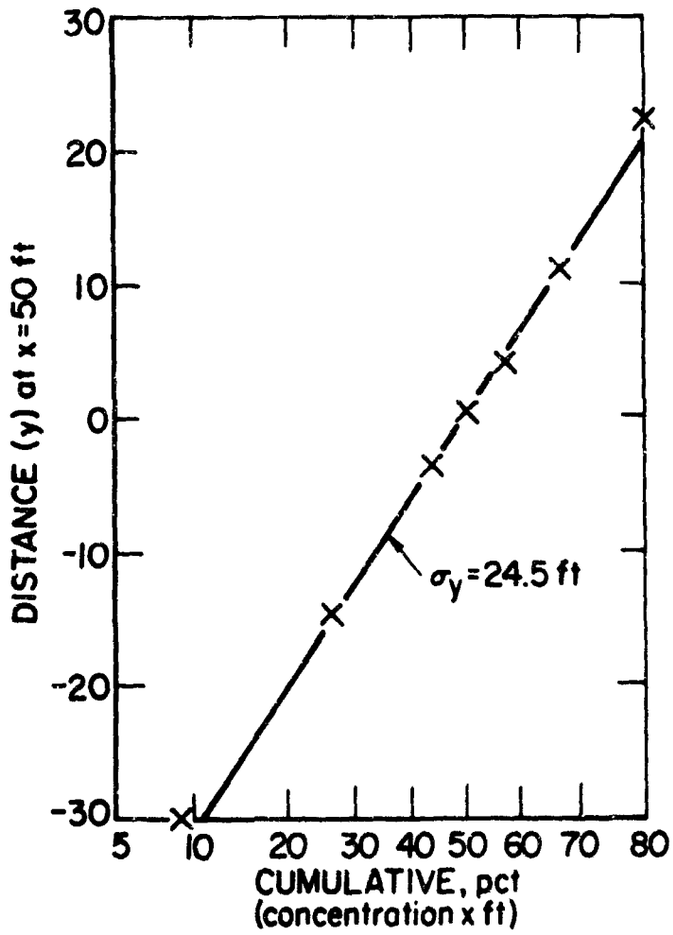

PX3-103
801

Figure 18. - Cumulative frequency distribution calculated from concentration data of test 11.

PRECEDING PAGE BLANK

ft/sec. By rearranging,

$$\sigma_z = \frac{100\ Q}{\pi \sigma_y \chi_{CL} \bar{U}} \qquad (13)$$

Using the six experiments with ambient temperature natural gas in which σ_y was derived from concentration measurements (table 5), σ_z was calculated as shown in table 6. In four of the six cases, the approximation $\sigma_z \approx \sigma_y$ is clearly justified. In the other two tests, numbers 2 and 11, the errors are compensating so that on the average $\sigma_z/\sigma_y = 1.01$. These results indicate that a good material balance was achieved in these tests and that the buoyancy of the natural gas had no effect on the dispersion.

In the case of a cold natural gas from evaporating LNG, the problem was more complicated because it was not possible to determine σ_y from the concentration data; primarily this was because some of the methane monitors at the 50 distance had been moved to 125 feet. Therefore σ_y had to be assumed to be given by x tan σ_θ as was proved for warm gas by the data of table 5. Also, the array of methane monitors was modified to give concentrations near water level, at a 10-foot elevation, and at a 15-foot elevation, all at 50 feet downwind from the source and near the expected centerline of flow. The vertical distribution of concentration during four tests with LNG is shown in figure 19. The upper solid line is the concentration distribution to be expected if $\sigma_z = 9$ feet; the lower dashed line shows the expected distribution at $\sigma_z = 3$ feet; seven of the eight significant measurements are between these extremes and the best estimate of σ_z in each test is 4 or 5 feet.

A test of the validity of this σ_z is provided by the experimental centerline concentrations and those obtained from equation (12). These data are presented in table 7. The experimental centerline concentration averages 26 percent above calculated, which means that one or both of the plume dimensions, σ_y and σ_z, were overestimated. Some part, but surely not all, of the 26 percent error could have arisen from the dimension of the evaporating LNG pool which is assumed here to be a point source.

6. Concentration as a Function of Distance. Our only pertinent data refer to measurements at 50 feet and 125 feet from the source. At these short distances, one should expect σ_y and σ_z to increase almost linearly with distance so that the familiar inverse square law should apply to concentrations. In figure 20, (10 minute) average concentrations at 50 feet are plotted against concentrations in the same direction from the source at 125 feet. The expected ratio of concentrations in each case is $(125/50)^2 = 6.25$ which is the sense of the correlating line.

PRECEDING PAGE BLANK

TABLE 5. - Observed and Calculated σ_y at 50 Feet from a Natural Gas Source

Test	Wind Speed, fps	σ_θ degrees	σ_y (obs.), ft	50 tan σ_θ, ft	$50\left(\frac{2.86}{\bar{U}}\right)$, ft
2&3	8.1	28.7	27	27.4	17.7
4&5	9.7	23.9	21	22.2	14.8
6	7.5	34.6	33	34.5	19.1
11	8.1	(28.7)[1/]	25	(27.4)	17.7

1/ Because of equipment failure, σ_θ is not available; estimated from tests 2 and 3 at the same wind speed.

TABLE 6. - Calculated Vertical Standard Deviation, σ_z Warm Gas, 50 Feet from Source

Test	Q ft^3/sec	χ_{CL}, %	σ_y, feet	σ_z, feet	$\frac{\sigma_z}{\sigma_y}$
2	5	.062	27	11.7	.43
3	20	.096	27	30.3	1.13
4	20	.172	21	18.3	.87
5	20	.150	21	20.9	1.00
6	20	.071	33	36.2	1.10
11	20	.081	25	38.8	1.55

TABLE 7. - Centerline Concentrations at 50 Feet in LNG Dispersion

Test	$\bar{U}$, fps	σ_θ	σ_y, ft[1/]	σ_z, ft	χ_{CL}, calc.	χ_{CL}, exp.
7	7.2	22.8	19	4	0.68	0.87
8	6.2	26.4	22	5	0.88	1.02
9	1.1	43.4	34	5	2.09	2.61
10	7.5	21.9	19	5	0.57	0.79

1/ Assumed to be given by 50 tan σ_θ (compare table 5).

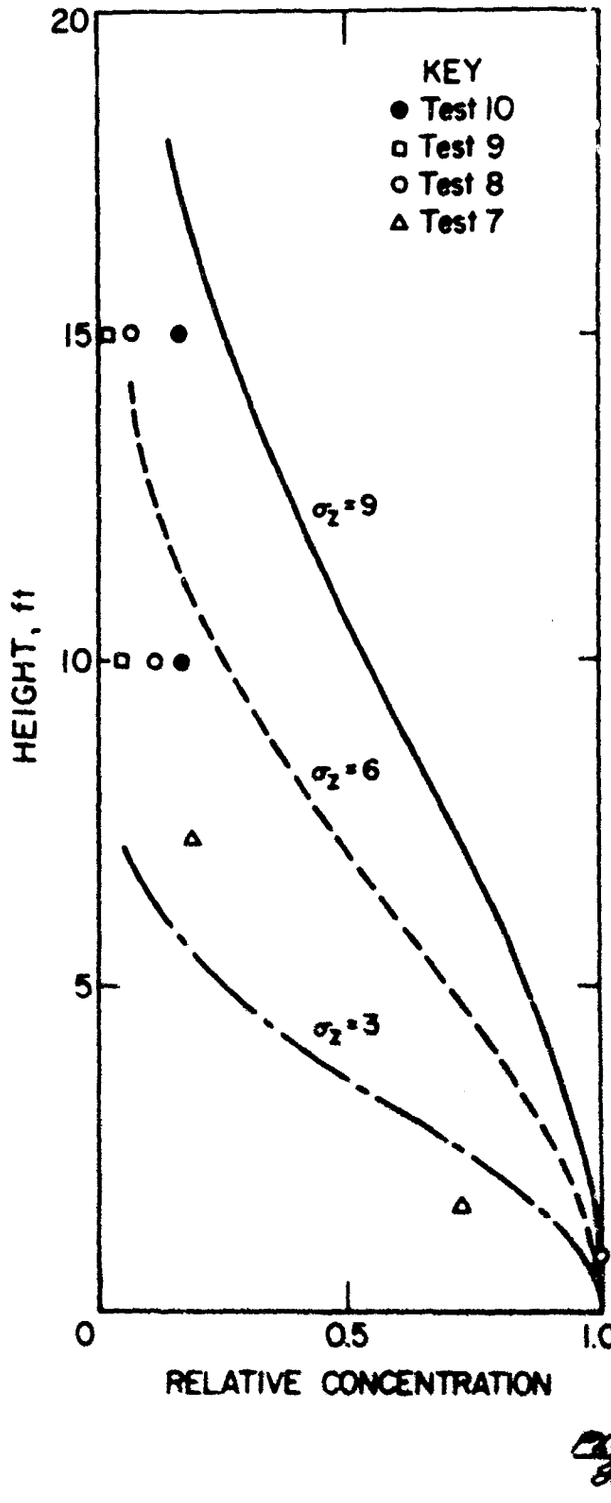

Figure 19. - Vertical distribution of concentrations at 50 ft from LNG source.

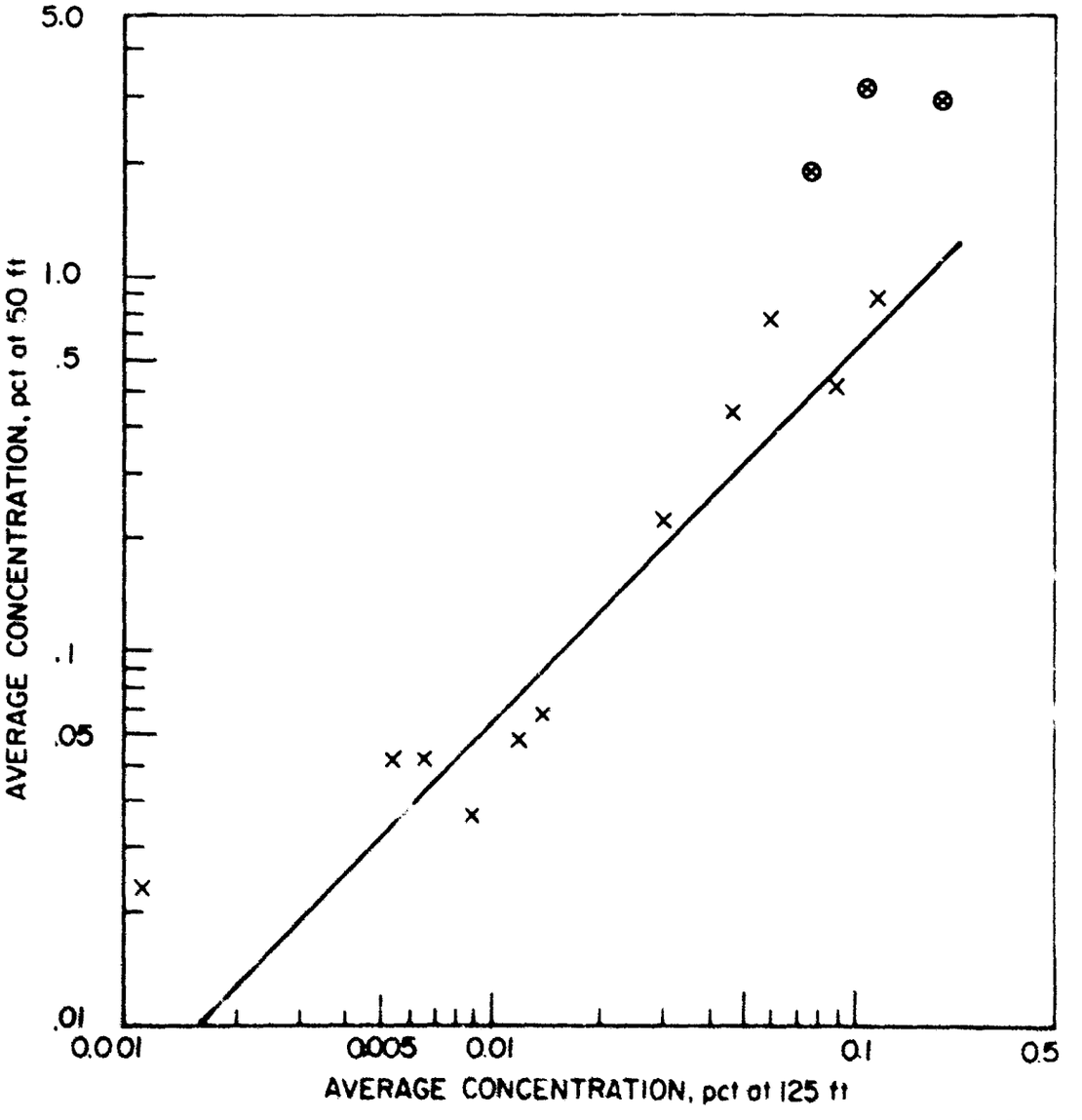

Figure 20. - Natural gas concentrations at 50 and 125 ft from source.

PRECEDING PAGE BLANK

This line fits most of the warm gas data and also those LNG (cold gas) data in which concentrations are less than one percent at 50 feet. When concentrations are several percent, downwind of an LNG spill, the inverse square law cannot be applied.[4/]

7. Peak-to-Average Ratios. Peak methane concentrations were determined directly from the records (e.g. figure 16) and average concentrations were obtained by use of a planimeter to measure total areas under the methane concentration curves for 10-minute intervals. The peak-to-average ratios at each of nine sample positions in test #7 (0.58 lbs LNG dispersed per second) are given in table 8. Two of the peak concentrations in column 3 are given as minimum values because the concentration transients went off-scale. Omitting these two data points, the average of all ratios is 12.4.

The average (all sensors) peak-to-average ratio for each of 9 tests is presented in table 9. The numbers fall clearly into two groups, around 20 for tests with warm gas and around 13-14 for tests with LNG. The same information is given in figure 21 wherein the straight line is drawn to represent ratios of 20. The sense of this figure is that transient flammable concentrations (greater than 5 percent) do not exist when the (10 minute) average concentration is less than 0.25 percent.

V DISCUSSION

A. Heat Transfer and Evaporation Rates

The most significant observation from our experiments is that LNG vaporizes at the very high rate of 0.037 lbs/ft^2 sec when poured onto water. When the spill is within a confined area, as in the aquarium experiments, a coherent sheet of ice forms under the LNG; as the ice thickens, it limits the heat flux to the LNG and the vaporization rate decreases with the inverse of the square root of time; in our experiments (figure 6) this change took effect imperceptibly at about 30-40 seconds.

If one must estimate the time-dependent heat flux through the ice layer, the general equation is

$$\frac{q}{A} = \frac{K\,(T_o - T_1)}{(\pi kt)^{1/2}} \qquad (14)$$

4/ The gas is presumably warm enough to disperse normally between 50 and 125 feet. But because of layering close to the source, the effective beginning of the dispersion is somewhere between 0 and 50 feet.

PRECEDING PAGE BLANK

TABLE 8. - Peak-to-Average Ratios, Test #7

Sensor	(angle)	Peak % CH_4	Average % CH_4	Peak/Average
1	(51)	0.86	0.041	21.0
2	(34)	>4.91	.436	>11.3
3	(17)	>6.35	.874	> 7.3
4	(8.5)	4.67	.769	6.1
10	(0)	6.08	.629	9.7
6	(-8.5)	6.67	.623	10.7
7	(-17)	5.13	--	--
8	(-34)	6.09	.736	8.3
9	(-57)	6.60	.356	18.5
				>11.6

TABLE 9. - Peak-to-Average Ratios, All Stations

Test	Gas	$(Peak/Average)_{av.}$
2	NG	16.3
3	NG	23.1
4	NG	15.0
5	NG	17.5
6	NG	28.0
		20.0
7	LNG	13.0
8	LNG	13.3
9	LNG	12.8
10	LNG	15.8
		13.7

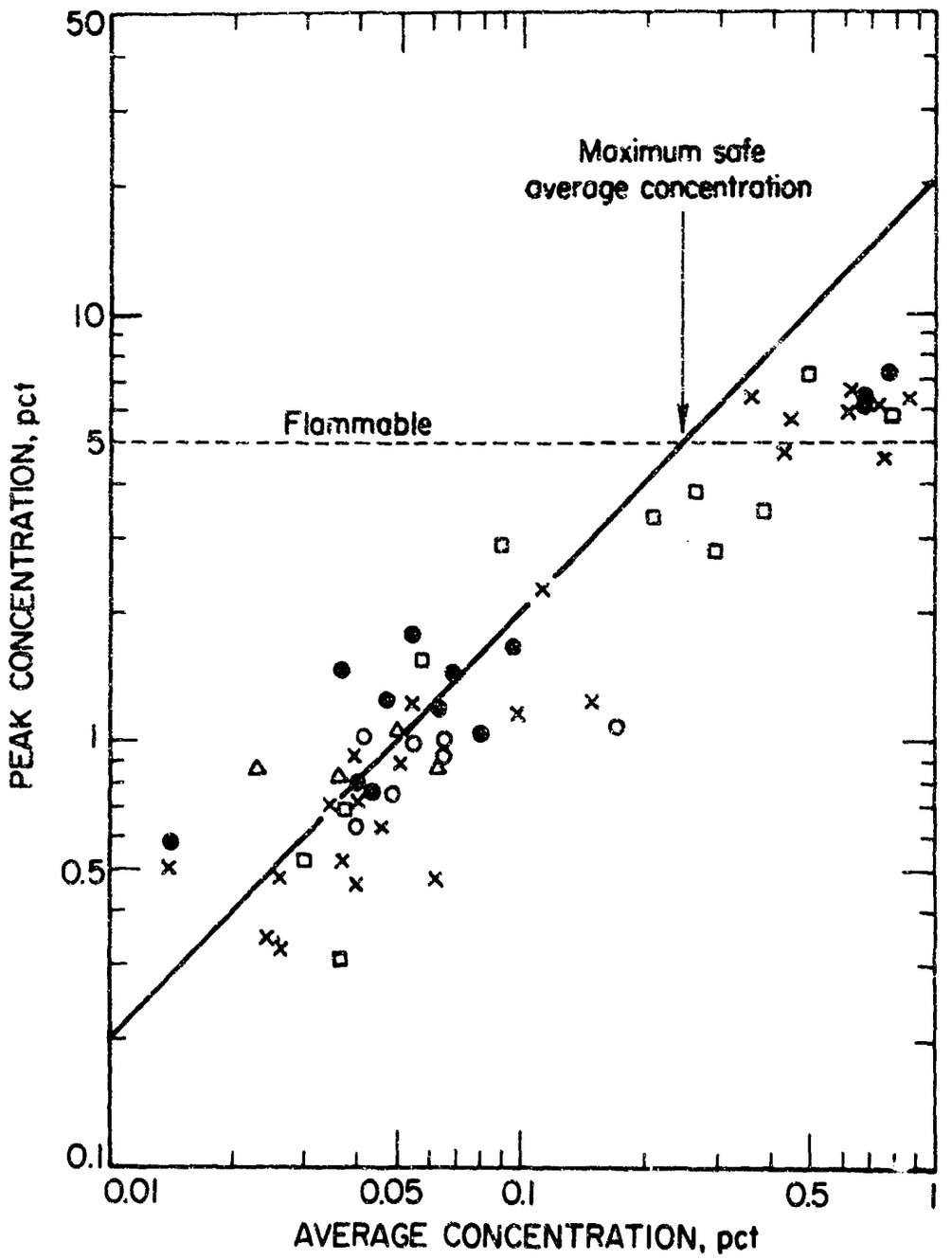

PX3-103
811

Figure 21. - Peak (3 seconds) and average (10 minutes) concentrations, 50 ft from a natural gas source.

This becomes awkward with ice because of the drastic variability of k (see table 2). If one defines a constant k by arbitrarily subtracting 20 seconds from each time interval (k' of table 2), one obtains

$$\frac{q}{A} = \frac{85000}{(t-20)^{1/2}} \text{ BTU/ft}^2 \text{ hr} \qquad (15)$$

which is equivalent to

$$\text{LNG vaporized} = \frac{0.095}{(t-20)^{1/2}} \text{ lb/ft}^2 \text{ sec} \qquad (16)$$

This overestimates the vaporization rate at short times, e.g. 0.095 lb/ft^2 sec at 21 seconds, but takes over properly at 28-30 seconds as shown by the dotted curve in figure 6. We had expected this time-dependent heat conduction through ice to be the most interesting and relevant aspect of the vaporization study.

As it turned out, no coherent ice floe was ever observed in our unconfined spills. When as much as 1?5 gallons LNG was poured onto the pond, water waves persisted throughout the vaporization as though the water under the LNG were in constant agitation. When approximately one pound LNG per second was released onto water over a 10-minute interval, the LNG pool assumed a roughly constant diameter. Had ice formed under the spill, the vaporization rate would have decreased from 0.037 lb/ft^2 sec at the beginning to 0.0039 lb/ft^2 sec at 10 minutes (equation 16) and the pool area would necessarily have increased tenfold.

Therefore we propose 0.037 lb/ft^2 sec as a time-independent rate, shown by a straight dashed line in figure 6. If this is in error, that is, if ice forms at some spillage rate beyond the scale of our experiments, the error is conservative. A point of incidental interest is that the burning rate of a pool of LNG (reference 1) is as much as 0.40 inch per minute which corresponds to .014 lbs LNG/ft^2 sec. This is only 40 percent of the vaporization rate on water and implies that the ignition of a vaporizing pool should have only a small effect on its rate of disappearance. This prediction was verified by one spill test in which the evolved vapors were ignited; the lazy flame which resulted was unable to burn back to the pool and remained in an unanchored blow-off condition. If one assumes that vaporization is maintained solely by heat transfer across the LNG-water interface (discounting, for example, exothermic hydration of methane as a contributing factor) then the heat flux must be 33,000 BTU/ft^2 hr. This figure is 3-4 times higher than expected and demands some comment on the possibility of experimental error.

The perimeter of the aquarium in which the vaporization experiments were carried out is 6 feet. The initial depth of LNG was 1.0-1.5 inches. Therefore there was an area of LNG-glass interface of 0.5-0.7 ft^2 in addition to the 2 ft^2 of LNG-water interface. Conceivably, this could

PRECEDING PAGE BLANK

account for an error of 25-35 percent in the figure for heat flux; however if heat transfer across an LNG-glass interface is normal for film boiling heat transfer (see below), then the maximum error from this source is reduced to the neighborhood of 5-10 percent. This is comparable to other experimental uncertainties such as losses by spattering and the effect of low temperature gases on the load cell.

Figure 22 combines the heat transfer studies of Merte and Clark[5/] on LN_2 and of Sciance, Colver and Sliepcevich[2/] on liquid methane. In each case the heat source was a conductive material such as an immersion heater. When either cryogen is brought into contact with a warm surface, the temperature difference is about 300° F; thus the initial heat flux should be about 6,000 BTU/ft^2-hr for LN_2 and perhaps 10,000 BTU/ft^2-hr for LNG. As the warm surface cools, the heat flux should decrease through a minimum which is about 2,000 BTU/ft^2-hr for LN_2 and something higher for LNG.

The observations here on LN_2 vaporization are in fair conformity with this picture. Figure 7b shows that when LN_2 is poured on ice the initial heat flux is indeed about 6,000 BTU/ft^2-hr. Thereafter it goes through a shallow minimum, although not as deep as indicated by Merte and Clark. However, the thermocouple record of figure 9 (which applies to a single point on the LN_2-ice interface rather than the whole 2 ft^2 surface) does show a deep minimum in heat transfer as evidenced by a severalfold change of slope.

On the other hand, LNG vaporization shows no evidence of film boiling; the apparent heat input is of the order of 30,000-40,000 BTU/ft^2 hr immediately after the completion of pouring. We think that a recent note by Manson[6/] may provide a partial explanation of this unexpected behavior. Manson observed that the minimum heat flux between LN_2 and a copper plate was 2,500 BTU/ft^2 hr. But when the copper was coated with a poorly conductive surface, 0.001 inch teflon, the minimum heat flux rose to 6,500 BTU/ft^2 hr. His explanation is the following: the vapor film between the cryogen and warm surface is not homogeneous in thickness; the underside of the cryogenic layer is in a standing wave with bubbles breaking loose at the antinodes (see figure 23); since the film thickness varies periodically at the antinode, so also does the heat flux from the warm surface; consequently a "cold spot" can appear on the surface if it is not too good a conductor, and the liquid can wet the surface; effectively the system is in transition between film and nucleate boiling even though the average temperature difference is consistent only with film boiling.

5/ Merte, H., Jr., and J. A. Clark. "Boiling Heat Transfer with Cryogenic Fluids at Standard, Fractional and Near-Zero Gravity." Trans. ASME, C, vol. 86, 1964, pp. 351-9.

6/ Manson, L. "A Periodic Nonuniform Heat-Transfer Mechanism in Film Boiling." Journal of Heat Transfer, February 1967, pp. 111-2.

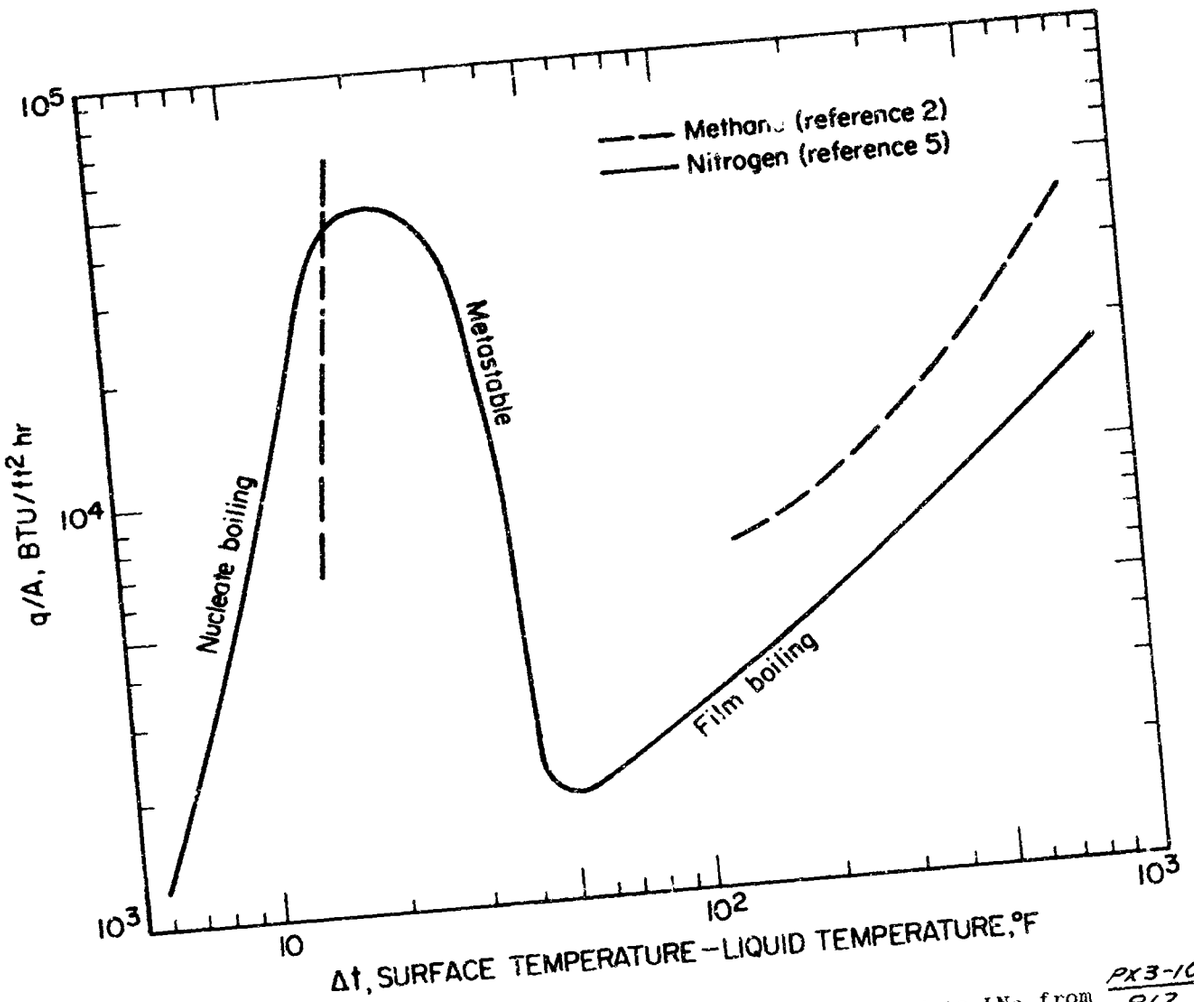

Figure 22. - Heat transfer rates to liquid methane and to LN_2 from conductive warm surfaces

PX3-103
8/12

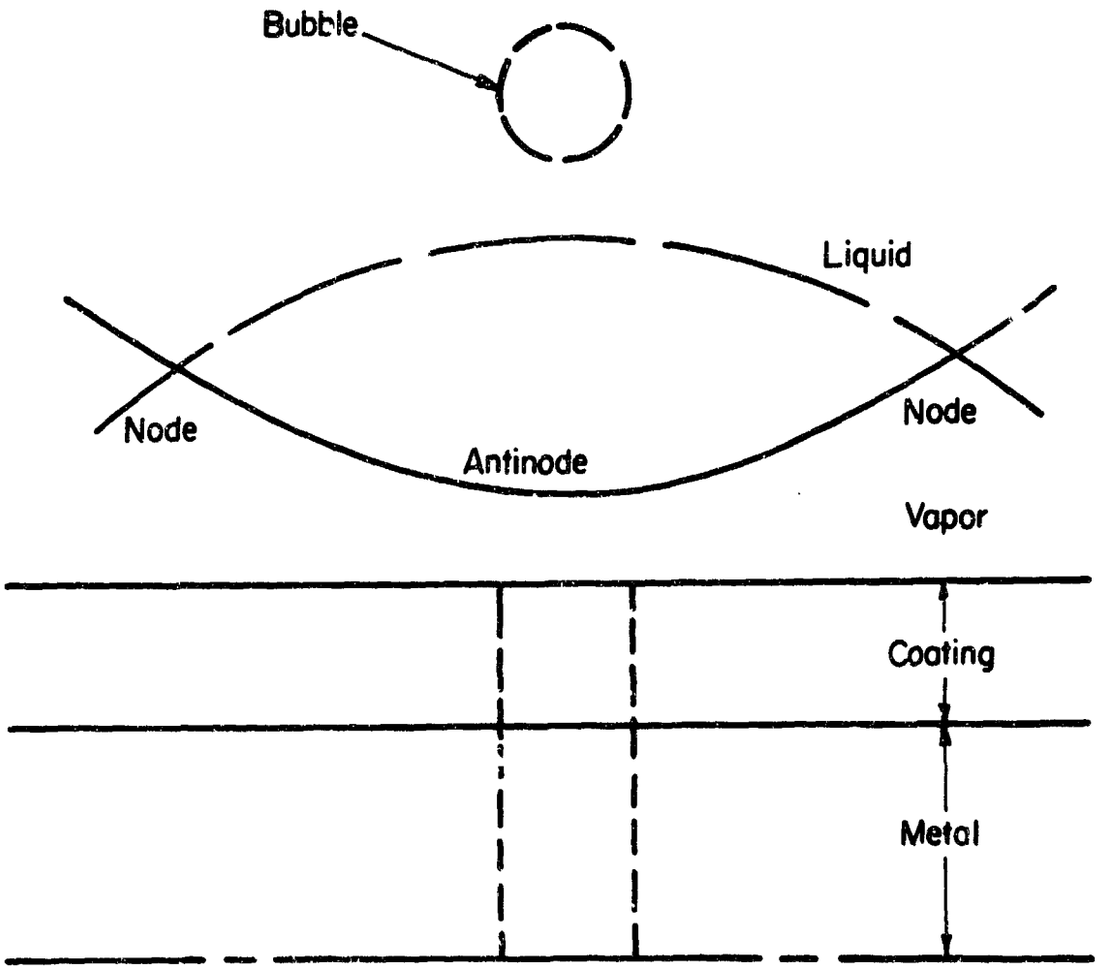

Figure 23. - Manson's model for periodic film boiling heat transfer.

PX3-103
794

PRECEDING PAGE BLANK

If Manson's postulate provides the proper mechanism for the high heat flux in LNG-water, we are still unable to explain why this occurs with LNG and not with LN_2-water.

B. Spreading of LNG on an Extended Water Surface

In terms of experimental considerations, this phase of the program and the empirical relationship

$$\text{max spill diameter} = 6.3\ W^{1/3}\ \text{ft} \qquad (7)$$

must be judged the least satisfactory. It was noted above that the LNG pool is seldom an ideal circle; also that there is an accumulation of LNG at the edge so that vaporization continues for some time after the LNG has disappeared from the center. Furthermore, we have no satisfactory explanation of why the leading edge of the spill should move outward at the same constant rate, 2.5 ft/sec, in all sizes of spill.

On the other hand, equation (7) derives a certain credibility from our intuitive acceptance of cube root scaling laws. If one considers how badly the equation could be in error, the worst possible case seems to be that spill diameter might vary with $W^{1/2}$ (because a diameter implies at least two dimensions). Fortunately, the measured maximum diameters of figure 12 provide a semi-independent check on equation (7). If one assume only that d_{max} vary with some power of W, the curve of best fit to the data is

$$d_{max} = 6.0\ W^{0.34}\ \text{ft} \qquad (17)$$

with a correlation coefficient of 0.97. The corresponding best empirical curve for duration of the pool is

$$\tau = 3.0\ W^{0.33}\ \text{sec} \qquad (18)$$

with a correlation coefficient of 0.94.

The diameter of a million gallon spill as predicted by equation (7) is 970 feet; by equation (17) it is 1040 feet. Our reservation about such predictions is not the inadequacy of present data but that a very large spill may develop an ice floe which would produce an upward bend in the extrapolation from our scale of experiment.

Putting together the vaporization rate

$$\frac{dW}{dt} = 0.18\ t^2\ \text{lb/sec} \qquad (4)$$

PRECEDING PAGE BLANK

and duration of vaporization

$$\tau = 2.5\ W^{1/3}\ \text{sec} \qquad (6)$$

one can predict the vapor evolution from any size of spill. Figure 24 deals with an instantaneous spill of 1000 gallons; supposedly the rate of vaporization from any size of spill increases along the same curve until terminated by depletion of the liquid in accordance with equation (6). Table 10 gives the maximum rates of vapor evolution in representative spills. The final column lists Q, the natural gas volume flow, which is used below in micrometeorological equations to predict gas concentrations downwind. The shape of the gas evolution curve in figure 24 is of some practical interest. In analyses of catastrophic failures of fixed installations it is typically assumed that cryogenic liquid immediately covers the entirety of a diked area; thus the transient begins with a spike followed by gradual lessening of vaporization rate, i.e., a mirror image of the curve in figure 24. The observer downwind of the assumed failure is first engulfed by a concentration peak followed by lesser concentrations which may or may not support flame propagation back to the spill. Such a prediction[7/] is reproduced in figure 25. But in a marine spill of LNG the downwind observer should encounter a gradually increasing methane concentration and have some warning of an impending flammable concentration; in many cases, depending on the size of spill, there is no problem of flashback to the spill area because the trailing edge of the concentration transient falls sharply toward zero.

C. Concentrations Downwind from a Natural Gas Source

In this part of the program, we have followed the concepts of Sutton[8/] and Pasquil[9/] which have been refined for experimental studies in this country by Cramer[10/] and Gifford,[11/] among others. Particular use has been made of the extensive meteorological and air pollution

7/ Welker, J. R., H. R. Wesson, and C. M. Sliepcevich. "LNG Spills: To Burn or Not to Burn." Presented at the Distribution Conference, Operating Section, American Gas Association, Inc., Philadelphia, Pa., May 12-15, 1969.

8/ Sutton, O. G. "Micrometeorology." McGraw-Hill Book Company, 1953.

9/ Pasquil, F. "The Estimation of Dispersion of Windborne Material." Meteorol. Mag., vol. 90, 1961, pp. 33-49.

10/ Cramer, H. E. "Engineering Estimates of Atmospheric Dispersal Capacity." Industrial Hygiene Journal, June 1959, pp. 183-189.

11/ Gifford, F. A. "Atmospheric Dispersion Calculations Using the Generalized Gaussian Plume Model." Nuclear Safety, vol. 2, 1960, pp. 56-9.

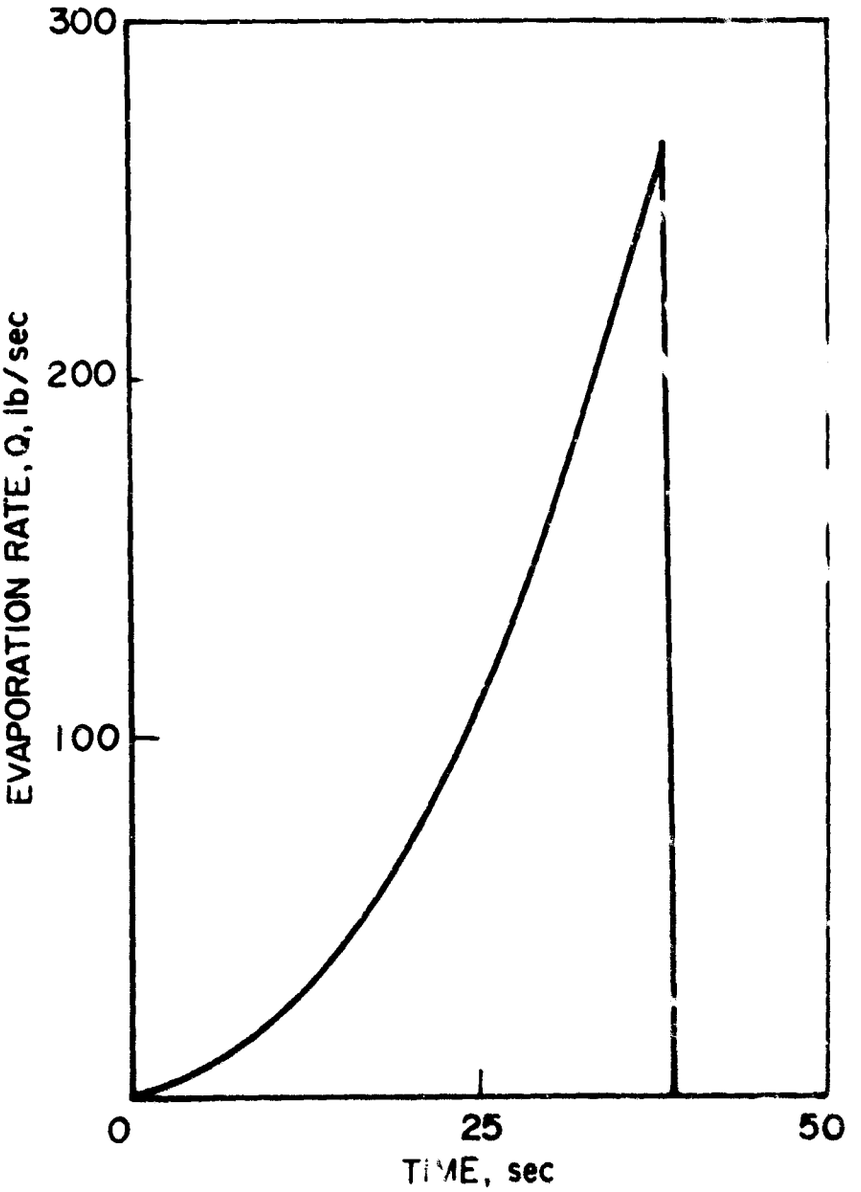

Figure 24. - Predicted vaporization rate, 1,000-gallon spill of LNG on water.

PN3-103
799

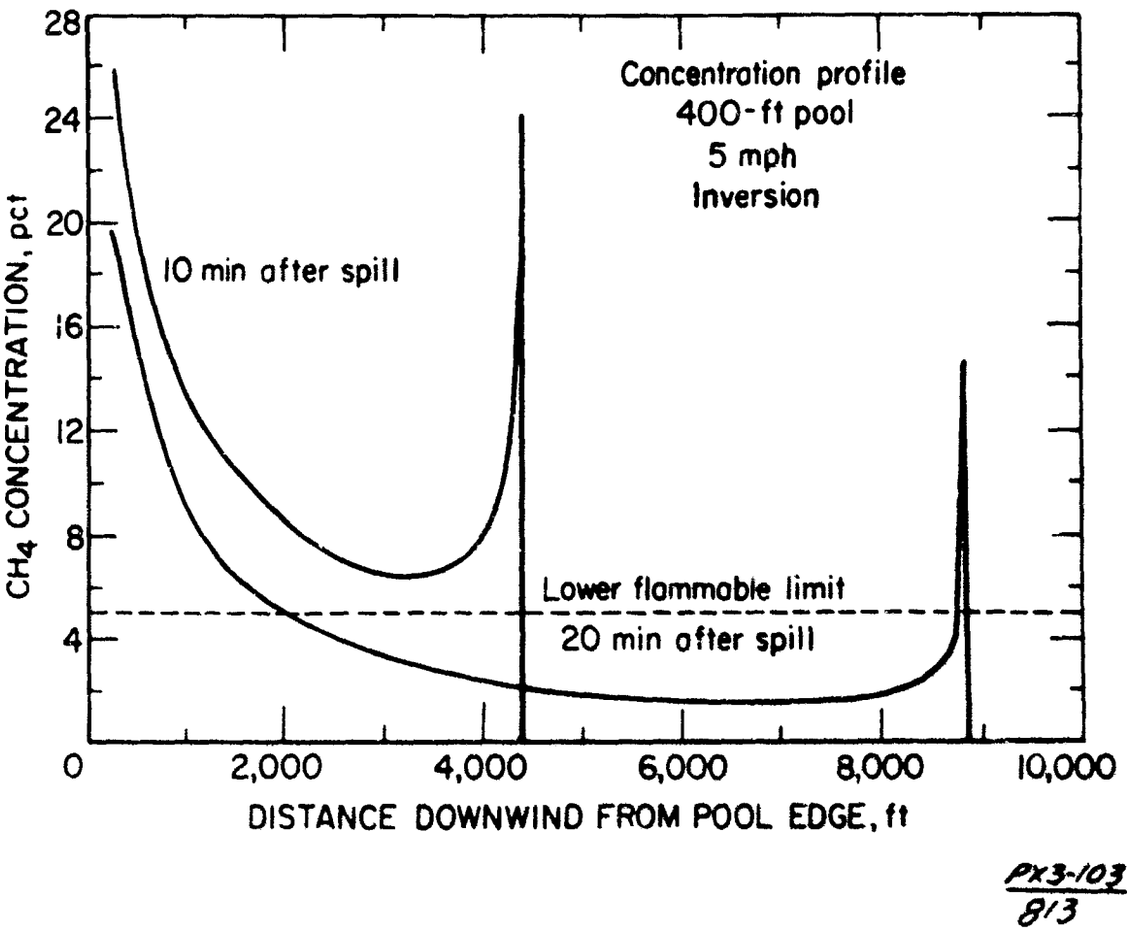

Figure 25. - Concentration profile downwind from an LNG spill into a diked area (from reference 7.)

PRECEDING PAGE BLANK

TABLE 10. - Calculated Vaporization Rates in Large Spills

Spill, gal	Size, lb	Duration, τ(sec)	Maximum Evaporation Rate lb/sec	Q(ft^3/sec)1/
100	380	18.1	59.4	1340.
1,000	3,800	39.0	277.	6210.
10,000	38,000	84.0	1285	28800.
100,000	380,000	181.	5940.	134000.

1/ Natural gas assumed to be methane, warmed by mixing to 0°C at 1 atm.

PRECEDING PAGE BLANK

data of Singer and Smith[3,12,13] which have been found to bear directly on this present problem.

With a sufficiently long sampling time such as 10 minutes, the average concentration $\chi(y,z)$ at any downwind distance x from an elevated source such as a smokestack is given by[10]

$$\chi = \frac{Q}{2\pi \bar{U} \sigma_y \sigma_z} \exp\left[-\frac{1}{2}\left(\frac{y^2}{\sigma_y^2} + \frac{z^2}{\sigma_z^2}\right)\right] \qquad (19)$$

where Q is the gas emission rate, $\bar{U}$ the average wind speed and σ_y and σ_z the standard deviations of concentration at distance x in horizontal and vertical directions, respectively. A top view of the plume is given in figure 26. Since we are presently concerned with a ground level source, z in equation (19) can have only positive values and all concentrations are doubled

$$\chi = \frac{Q}{\pi \bar{U} \sigma_y \sigma_z} \exp\left[-\frac{1}{2}\left(\frac{y^2}{\sigma_y^2} + \frac{z^2}{\sigma_z^2}\right)\right] . \qquad (20)$$

Finally, since we are concerned with maximum hazards, the important concentrations are those on the centerline of average flow

$$\chi_{CL} = \frac{Q}{\pi \bar{U} \sigma_y \sigma_z} . \qquad (12)$$

From the above equation and from figure 26 it is clear that the crucial matter is the assignment of values to σ_y and σ_z. At very short distances (see figure 26) σ_y varies directly with x and at very long distances with $x^{0.5}$; at the intermediate distances which are of interest in air pollution, σ_y varies with x to some exponent between 0.5 and 1.0; some useful values are given in table 11, derived from reference 13. Note that under unstable and neutral atmospheric conditions $\sigma_z \approx \sigma_y$, while under stable conditions (inversion) $\sigma_z < \sigma_y$.

12/ Singer, I., K. Imai, and R. del Campo. "Peak to Mean Concentration Ratios for Various Terrain and Vegetation Cover." J. Air Pollution Control Association, vol. 13, 1963, pp. 40-42.

Singer, I. "Relationship between Peak and Mean Concentrations." J. Air Pollution Control Association, vol. 11, 1961, pp. 336-341.

13/ Singer, I., and M. Smith. "Relation of Gustiness to Other Meteorological Parameters." J. of Meteorology, vol. 10, 1953, pp. 121-6.

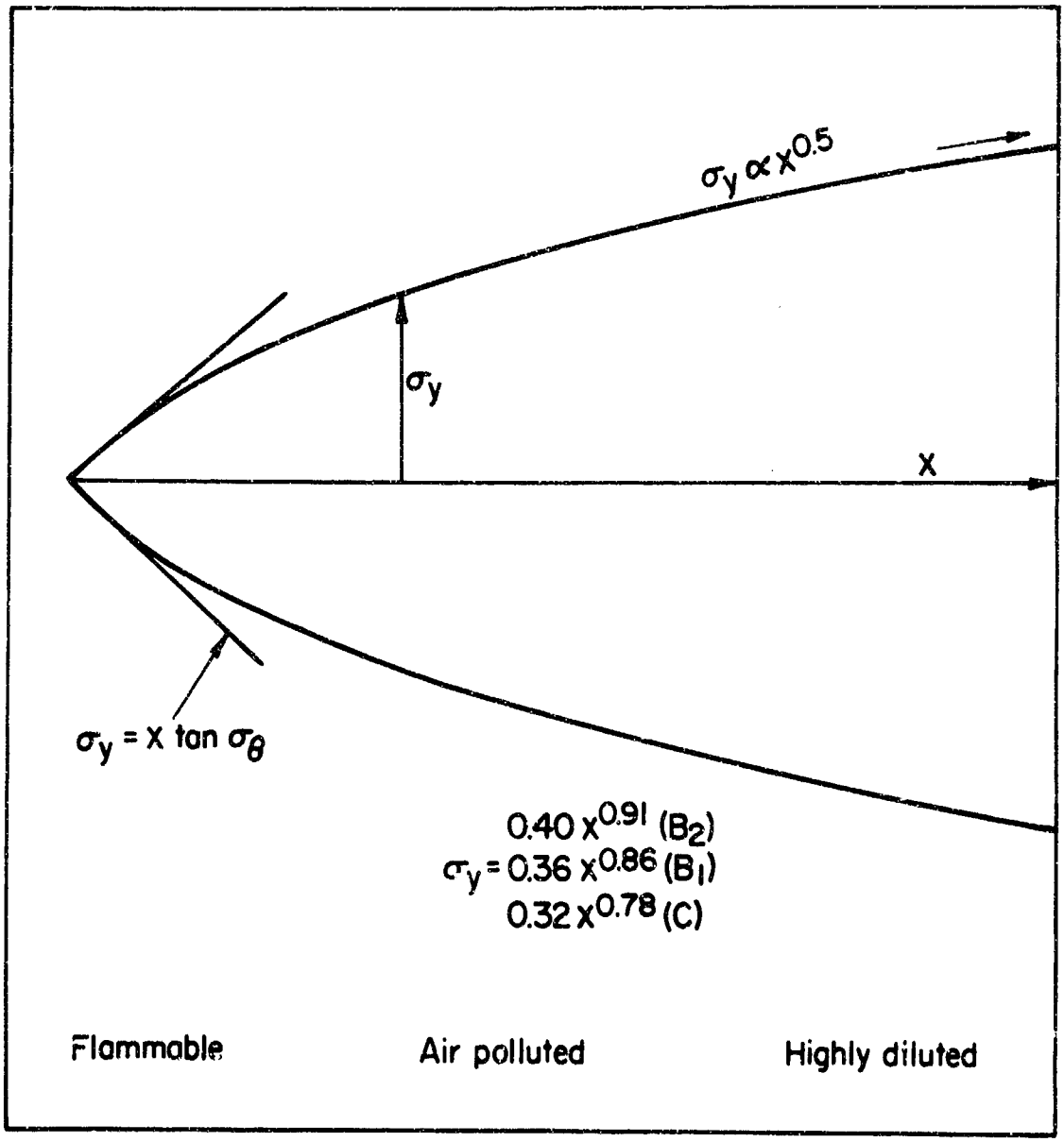

Figure 26. - Plume extending downwind from a spill.

PX3-103
8/5

TABLE 11. - Some Representative Atmospheric Conditions[1/]

Gustiness Classification		Fluctuation of Horizontal Wind Direction	Frequency of Occurrence Percent of Time	Wind Speed ft/sec		Plume Dimensions	
				Mean	σ	σ_y	σ_z
A	extremely unstable	>90°	1	5.9	3.6	--	--
B_2	unstable	45-90°	3	12.4	5.9	$0.40\ x^{0.91}$	$0.41\ x^{0.91}$
B_1	unstable	15-45°	42	22.8	10.0	$0.36\ x^{0.86}$	$0.33\ x^{0.86}$
C	neutral	>15°	14	35.0	10.0	$0.32\ x^{0.78}$	$0.22\ x^{0.78}$
D	stable	<15°	40[2/]	Depends on height of inversion		$0.31\ x^{0.71}$	$0.062\ x^{0.71}$

1/ Taken from reference 13 and other publications of the Brookhaven National Laboratory. Refer to two years' data, 355 feet aboveground.

2/ Primarily a nocturnal phenomenon.

PRECEDING PAGE BLANK

No attempt has been made here to add to the great body of general information in micrometeorology. The present problem raises special questions related to natural gas as a pollutant.

(1) The pertinent concentration, χ, is the lower flammable limit, 5 volume percent, rather than some concentration given in parts per million. Therefore we are interested in plume dimensions, σ_y and σ_z, close to the source rather than far downwind.

(2) Equations (12) and (20) refer to time-averaged concentrations resulting from a continuous source (or alternatively, χ is given in units of dosage, concentration x time, when Q is a total volume of gas emitted). But our interest is in peak concentrations which may be instantaneously flammable.

( ) The natural gas evolved from an LNG spill is cold enough to be heavier than air. Therefore it must "layer" to some extent (σ_z is suppressed) until it has warmed sufficiently to become buoyant.

1. Concentrations Close to the Source. The experimental finding (col. 4 and 5 of table 5) is that σ_y is given in good approximation by x tan σ_θ (this is also evident from figure 26). Whenever σ_y and σ_z are equal (tables 6 and 11) equation (12) may be rewritten

$$\chi_{CL} = \frac{Q}{\pi \sigma_y \sigma_z \bar{U}} = \frac{Q}{\pi x^2 \tan^2 \sigma_\theta \bar{U}} = \frac{Q \bar{U}}{\pi x^2 \tan^2 \sigma_\theta \bar{U}^2} \cdot \qquad (21)$$

For small angles, σ_θ (radians) $\approx$ tan σ_θ so that

$$\chi_{CL} = \frac{Q \bar{U}}{\pi x^2 \sigma_\theta^2 \bar{U}^2} \cdot \qquad (22)$$

But the sense of figure 14 and equation (9) is that $\sigma_\theta \bar{U}$ is essentially constant for unstable and neutral conditions with a value of about 2.86. Therefore

$$\chi_{CL} \approx \frac{3.89\ Q \bar{U}}{x^2} \text{ volume percent} \cdot \qquad (23)$$

This equation illustrates several important points. First, the concentration varies with the inverse square of distance (see also figures 17 and 20). More significantly, it shows that concentration at a given distance is directly proportional to wind speed, $\bar{U}$. This point is not explicitly obvious in such equations as (19) and (20) which have generally been interpreted to mean that concentration varies inversely with wind speed. The dependence of concentration on wind speed is less easily demonstrable at long distances or under inversion conditions.

A nomograph of equation (23) is given in figure 27 to facilitate its use. For example, if we wish to determine the average centerline concentration 50 feet downwind of a 20 ft^3/sec source in a 6 ft/sec wind, we first construct a straight line between U = 6 and x = 50 (step 1). Next, construct a straight line from the intersection point of the first straight line and the vertical line labeled $\alpha = \frac{U}{x^2}$ and point Q = 20 (step 2). This line intersects the χ_{CL} axis at a predicted average concentration of 0.19 volume percent natural gas (or methane). In practice, we should expect the actual average value to be somewhat less than this because the produce $\sigma_\theta . \overline{U}$ appears to be somewhat higher at water level than 2.86 (figure 14); estimates obtained by the use of figure 27 were found to be conservative.

At distances beyond those investigated here, where flammable concentrations may still be expected with very large Q we should expect to find

$$\chi \alpha \frac{1}{x^p} \qquad (24)$$

where $1.5 \leq p \leq 2.0$. Thus if we use Singer's and Smith's results for a B_2 gustiness condition and take $\sigma_y = 0.4\ x^{0.91} = \sigma_z$, then

$$\chi_{CL} = \frac{100\ Q}{\pi\ \sigma_y \sigma_z\ \overline{U}} = \frac{100\ Q}{\pi\ (0.16)\ x^{1.82}\ \overline{U}} = \frac{199\ Q}{\overline{U}\ x^{1.82}} \text{ volume percent.} \qquad (25)$$

A nomograph of this equation is given in figure 28. Centerline concentrations can be determined by use of the procedure given for figure 27. Conversely, both figures can be used in a reverse sequence to determine the conditions that could lead to a particular average combustible concentration. For example, the critical distance at which a specific concentration exists is readily found for any Q-$\overline{U}$ combination; alternatively, the critical feed rate (Q) can be found for any $\overline{U}$-x combination, and the critical wind speed ($\overline{U}$) can be found for any Q-x combination.

If natural gas were released over an extended area (as from an LNG leak below water) we could use the above analysis as a first approximation, if distances were measured from the center of the released zone. In general, except with extended sources along the centerline, we should expect the results obtained from figures 27 and 28 to be conservative estimates of the actual concentrations. Further, concentrations above and on either side of the centerline would also be less than those calculated by the use of equation (20). A computerized method of allowing for area of the source is described in reference 14.

14/ Parker, R., and J. Spata. "Downwind Travel of Vapors from Large Pools of Cryogenic Liquids." Proceedings of the First International Conference on LNG, April 7-12, 1968. Edited and produced by Institute of Gas Technology, Chicago, Illinois.

2. Ratios of Peak Concentration to Average Concentration. If a methane sensor were mounted near a steady natural gas source, the peak concentration and average concentration would be identical. Also, some miles downwind where complete mixing had occurred, peak and average concentrations would again be equal. But at intermediate distances, the ratio of peak to average concentration goes through a maximum. This ratio is evidently a function of gustiness[12] as well as of distance and of concentration.

In air pollution studies there is support for a semi-theoretical law that a centerline concentration varies with the duration of its measurement by

$$\chi_{CL} = kt^{-0.2} \quad . \qquad (26)$$

Thus, the "peak" which might be measured over a 3-second interval is $\left(\frac{600}{3}\right)^{0.2}$ or 2.9 times the concentration averaged over a 10-minute interval. However, experimental ratios of peak-to-average have often been higher.

The results for pipeline gas in figure 21 where the peaks are typically about 1.0 percent, and averages about 0.05 percent give ratios of 20:1 which are larger than anything we have encountered in the literature. But if one considers only those results where the peak concentrations are flammable (cold gas), then a ratio of 20 seems to be a safe upper limit. Put another way, in the present study we never encountered a flammable (5 percent) peak when the (10 minute) average concentration was less than 0.25 percent. Thus, the critical concentration to be looked for in the nomographs (figures 27 and 28) should be 0.25 percent rather than 5.0 percent. Also, if one uses an air pollution equation to calculate concentration distributions such as those in figure 25, the plume is not safe against flashback even though the concentration dips below 5.0 percent.

3. Cold Gas Layering. The release of a cold, heavier-than-air gas (as from LNG) near the surface of a body of water creates a problem quite similar to that of a temperature inversion. If the gas spreads out only in the horizontal direction, the gas concentration must vary as

$$\chi \alpha \frac{1}{\sigma_y} \text{ or } \frac{1}{x^p} \qquad (27)$$

where p is the exponent given in table 11 and has values $0.5 \leq p \leq 1.0$. But in reality there is always some vertical dispersion. Note that in table 11 (stable) the $\sigma_y\sigma_z$ product is proportional to $x^{1.42}$ while

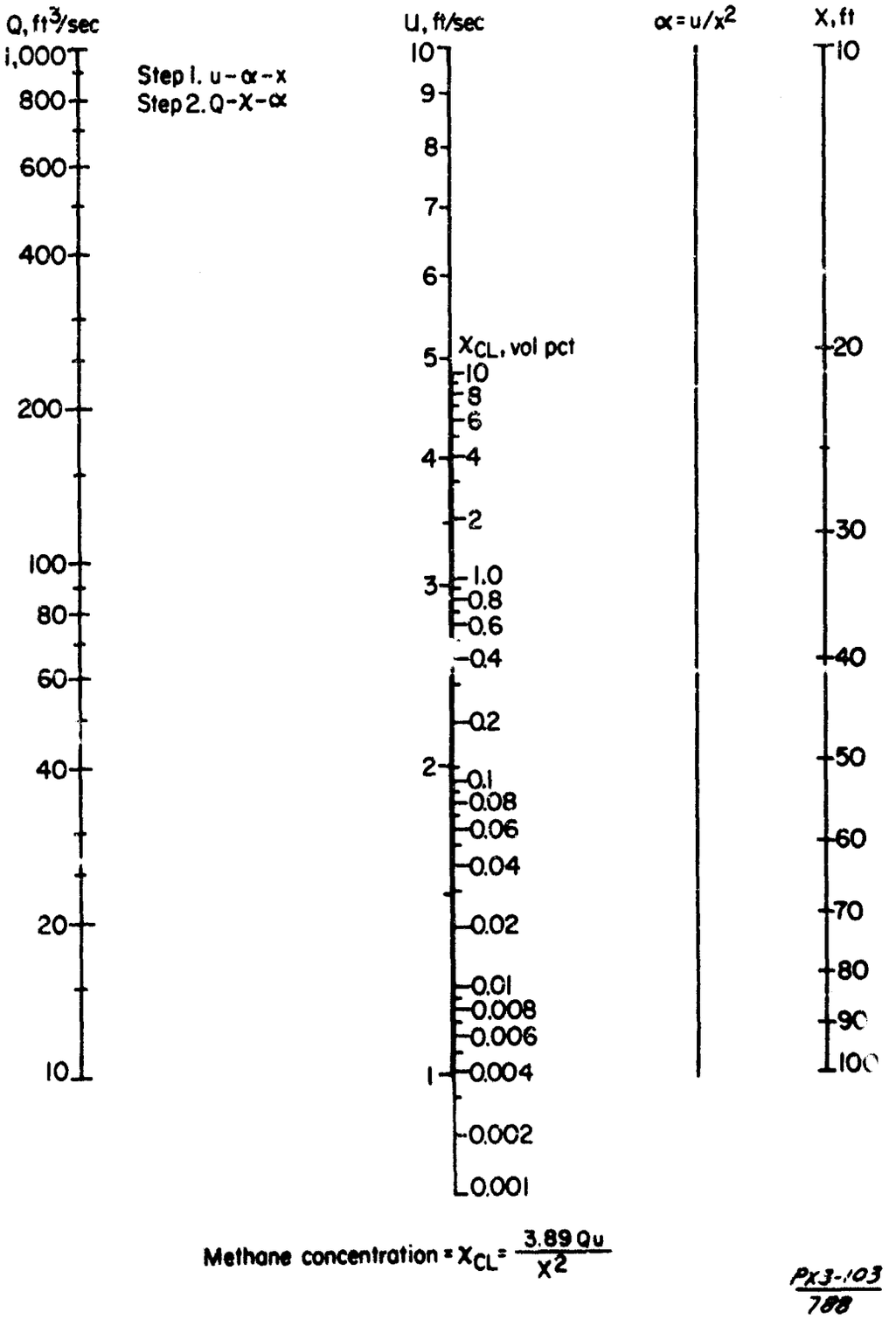

Figure 27. - Nomograph pertaining to concentrations near a small natural gas source.

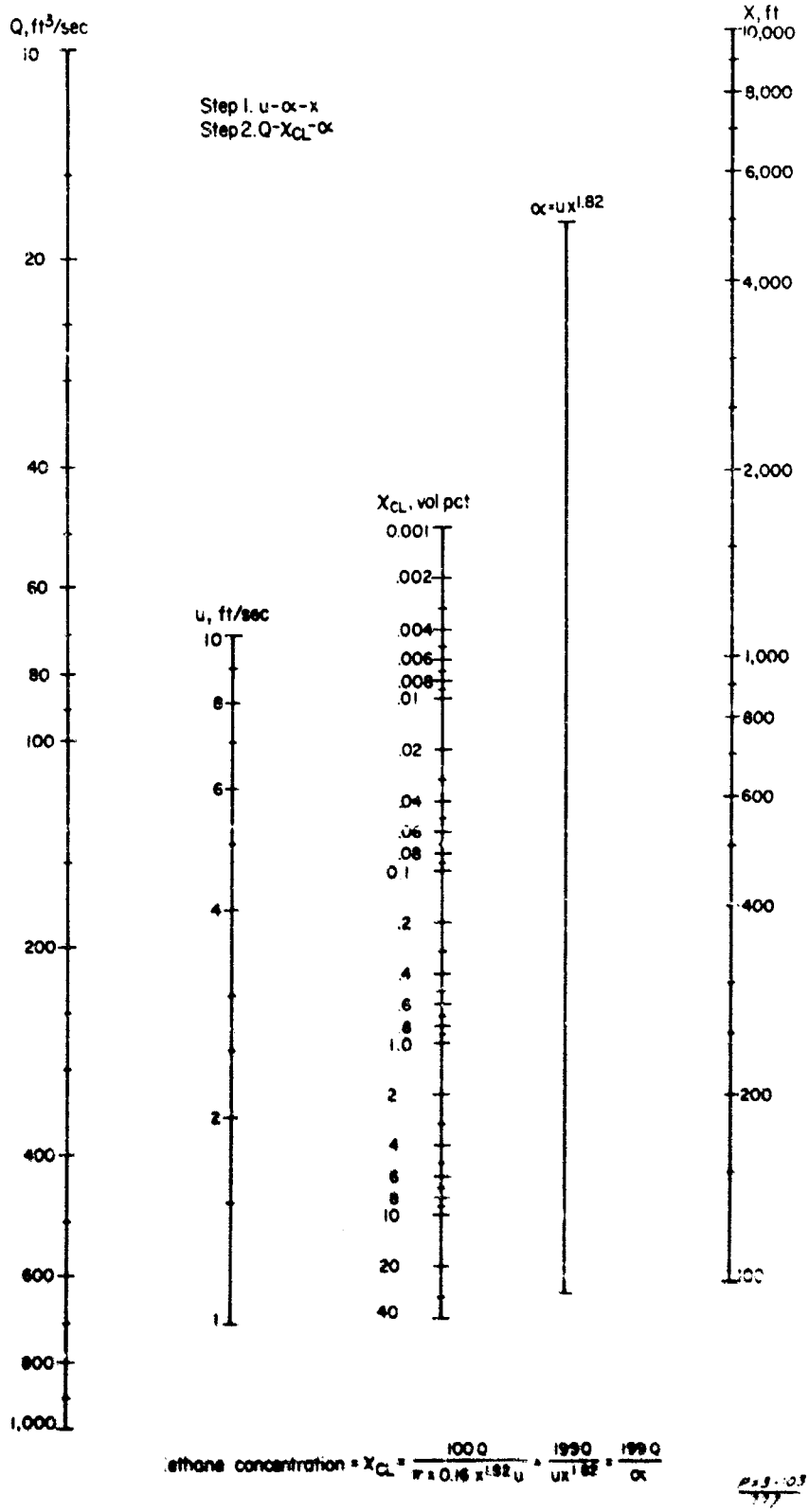

Figure 28. - Nomograph pertaining to concentrations at long distances from a natural gas source.

PRECEDING PAGE BLANK

Cramer[10] proposes $x^{1.3}$ for strong inversions. We should expect to find something comparable for the distance over which LNG vapors form layers.

The significant finding of our experiments is that layering does exist over approximately the distance that the LNG vapor trail remains flammable, in other words, over the distance that is relevant for predicting hazard.

The values of σ_z at x = 50 feet were 4 and 5 feet in the four experiments of table 7. Roughly, $\frac{\sigma_z}{\sigma_y} \sim 0.2$ and this leads to two interpretations which yield the same conclusion. Since $\sigma_y \approx x \tan \sigma_\theta$ at our short distances, we may argue that

$$\sigma_z \approx (0.2 \tan \sigma_\theta)\, x \qquad . \qquad (28)$$

Functionally, this is identical to the result shown for stable conditions in table 11. Or alternatively, we can say that

$$\sigma_z \approx x^{0.6} \tan \sigma_\theta \qquad (29)$$

which gives a $\sigma_y \sigma_z$ product proportional to $x^{1.6}$ at short distance. At longer distances, this should come into agreement with the Cramer and Singer and Smith values.

Based on these admittedly scanty results, our suggestion is that layering be treated exactly as one treats a temperature inversion. This is essentially the procedure followed in reference 7.

D. Explosion Hazard (Without Ignition)

The most serious question involving maritime transport of LNG is whether the small-scale explosions which were observed in this program could scale up to damaging dimensions in the case of a real accident. To even discuss this issue, it is necessary to classify the observed explosions into at least two, and possibly three, catagories:

1. The small "pops" associated with the shattering of individual small aggregates of ice. No hazard is thought to exist by reason of these little explosions. A video tape of test 13 (about 1 lb LNG/sec for 600 sec) was rerun to count the frequency of these incidents with the result shown in figure 29. There was very little audible activity during the first minute, and it required at least 2-3 minutes for the "popping" to reach its ultimate frequency of 1-2 per second.

PRECEDING PAGE BLANK

2. The acceleration of this rate of "popping" to a staccato climax as though perhaps a dozen small explosions were affecting each other by proximity. This occurred several times; water was thrown upward about 10 feet and the steel drum which was suspended 18 inches above the water was rattled about but not deformed.

3. The larger-scale incident shown in figure 5. From observers' reports, this explosion might have been equivalent to a stick of dynamite. The delay time to this explosion was not more than 1/8 second. The aquarium accident, which may have been of the same type but on a smaller scale occurred at the conclusion of pouring of the LNG or about 3.2 seconds after first LNG-water contact.

We have given consideration to several candidate explanations for these explosions. The rationalization that comes immediately to mind is the entrainment of LNG within an envelope of ice. There is considerable precedence for this idea in the history of molten metal-water explosions[15/] which have occasioned concern in the design of nuclear reactors; also in the literature of molten Kraft smelt-water explosions[16/] which have occurred in the paper industry. In the problem areas above, it has been postulated that liquid water gets entrapped in a high temperature matrix and is rapidly vaporized until it fragments the confinement because of the resultant steam pressures. In the same way, one might expect LNG to become encapsulated in ice. This seems to fit the observations of the "pops" described above: many small ice particles; some of these emitting jets of white vapor; some of these latter disappearing after appreciable time delay with audible reports.

The inactivity of LN_2 in comparable spills may be related to some of these observations from the molten metal-water study as discussed in reference 15; the surface tension of aluminum was lowered by adding bismuth and "greater tendency toward fragmentation ... resulted"; the viscosity of the water was increased and the "fragmentation of lead, tin and bismuth was greatly reduced"; the systems of greatest density difference, e.g. lead-, tin- and bismuth-water, show "generally more fragmentation" than those of lower density difference, such as aluminum- and zinc-water. However, when the water temperature was increased to 100° C (and when the water was replaced by LN_2) there was "no fragmentation whatever, giving evidence ... that metals will not fragment in a saturated liquid". Contrary to this last observation, our low temperature fluid, LNG, must have been nearly a "saturated liquid".

A second postulate of some attractiveness is that LNG hydrates are in some way involved. If hydrates can form at the appropriate rate in

---

15/ Brauer, F. E., N. W. Green, and R. B. Mesler. "Metal/Water Explosions", Nuclear Science and Engineering, vol. 31, 1968, pp. 551-4.

16/ Nelson, W., and E. A. Kennedy. "What Causes Kraft Dissolving Tank Explosions". Paper Trade Journal, July 15, 1965, pp. 50-56.

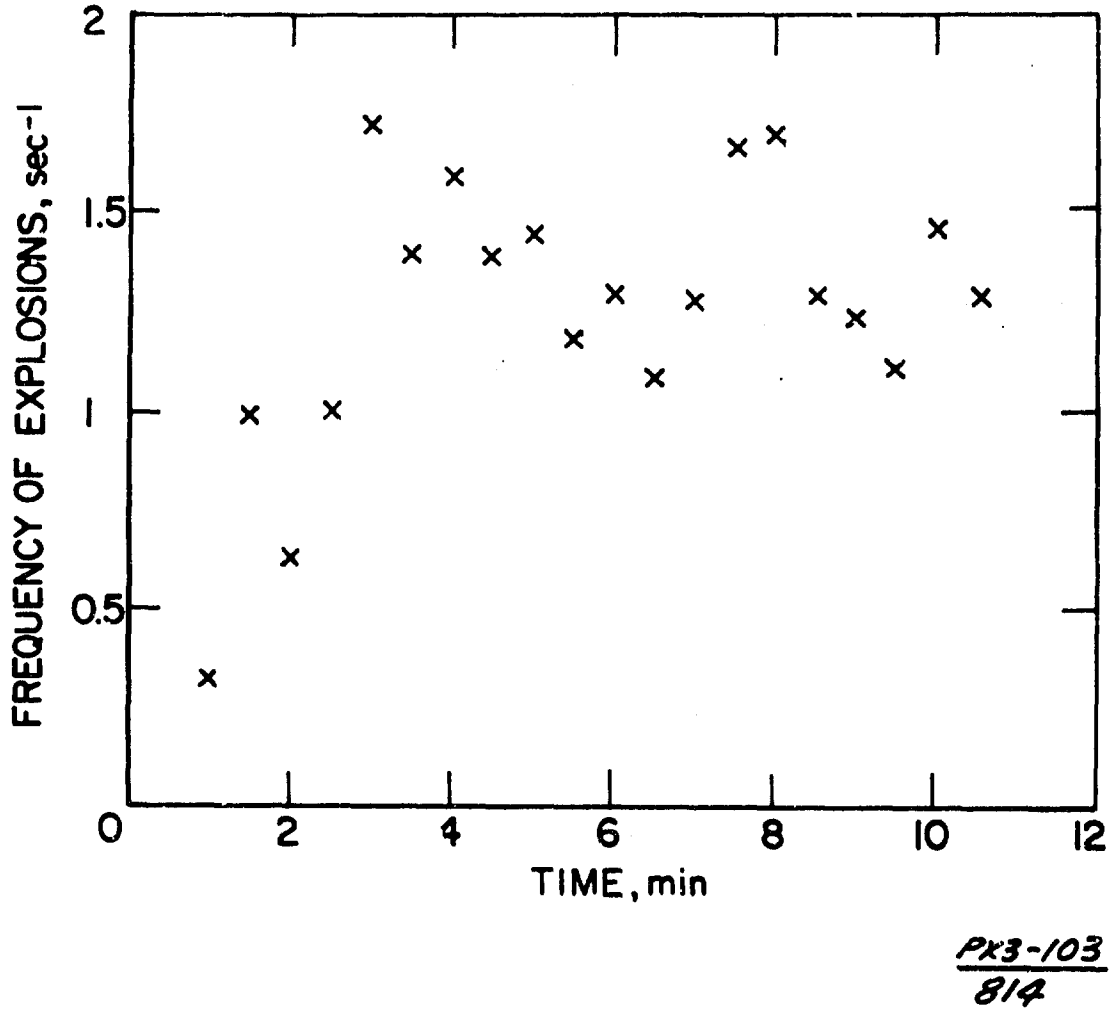

Figure 29. - Frequency of small-scale explosions in LNG dispersion test, one lb/sec LNG poured onto water.

the LNG-water system, the vapor pressure will be drastically reduced and the encapsulation very much facilitated. The decomposition pressures of methane hydrate, 8 $CH_4 \cdot 46\ H_2O$ and of ethane hydrate, 6 $C_2H_6 \cdot 46\ H_2O$, are about 25 atm and 4 atm, respectively at 32° F.[17] Moreover, the formation of 8 $CH_4 \cdot 46\ H_2O$ from methane and water is exothermic by about 15 kilocalories per mole of methane;[18] a sudden hydration of about 1/4 pound of methane could account for the energy release of the largest observed explosion. Also, the unusual boiling rate of LNG on water suggests an unusual interfacial attraction of LNG for water.

On the other hand, we know of no evidence whatever that LNG hydrates can form at any substantial rate. Structurally, the methane hydrate is said to be a clathrate;[19] the aggregate of 46 water molecules contains two "holes" of 5.1 Angstrom diameter and six "holes" of 5.8 Angstrom diameter; methane molecules can inhabit each of these eight cavities but ethane molecules can penetrate only the larger six. The nature of these hydrates almost dictates that they be formed from the vapor phase. If one cools the system with an excess of LNG, one should increase the stability of the hydrates but at the same time the available water vapor is diminished.

When 15 grams of water was placed in a stationary autoclave at 49° F with an atmosphere of methane at 1100 psi, very little reaction was observed in 7-1/2 hours; when the autoclave was rotated and the contents mixed with steel bearings, 90 percent of equilibrium conversion was attained in three hours.[19] These are hardly the reaction rates that one associates with explosions.

About a man-week was spent in preliminary attempts to form hydrates by adding LNG to liquid water with various degrees of agitation; all results were negative. The underwater release of 5 gallons of LNG by opening the container explosively was in the same category of experiment; the only evident result was the fast evolution of a bubble of natural gas; no secondary explosions were detected.

Nonetheless, if the subject of LNG explosions is to be followed up, some study of the kinetics of hydrate formation is indicated.

17/ Nagata, I., and R. Kobayashi. "Prediction of Dissociation Pressures of Mixed Gas Hydrates from Data for Hydrates of Pure Gases with Water". I&EC Fundamentals, vol. 5, 1966, p. 466.

18/ Institute of Gas Technology Research Bulletin No. 1 "The Storage of Natural Gas Hydrate" by J. D. Parent, quoting de Forcrand and Hammerschmidt. Ind. Eng. Chem., vol. 28, 1935, p. 851.

19/ Galloway, T. J., W. Ruska, P. S. Chappelear, and R. Kotayaski. "The Experimental Measurement of Hydrate Numbers for Methane and Ethane and Comparison with Theoretical Values". Submitted for publication in Industrial and Engineering Chemistry Fundamentals, February 25, 1969.

PRECEDING PAGE BLANK

The photographs of figure 5 suggest a more simple explanation for this one incident. The LNG pool seems unnaturally quiet in the first three frames and one wonders if this is not an ordinary "bump" from superheating. Such problems have frequently been observed with cryogens in dewars.[20/] If bubbles failed to form during 1/8 second, there would be no vapor film and heat transfer to the LNG could attain at least the highest value shown for nucleate boiling in figure 22, of the order of 10^5 BTU/ft^2 hr; this is about 4 BTU, or the equivalent of 1 gram TNT through each square foot of contact surface during the delay period.

But contrary to this simple mechanism, the LNG appears milky white in the photographs as though it had formed many bubbles in pouring over the lip of the container.

VI CONCLUSIONS AND RECOMMENDATIONS

From the handling of about 2,000 gallons LNG as described above, we have reached several conclusions pertaining to the spillage of LNG on water:

1. Vaporizing pools of LNG spread to a maximum diameter (in feet) which is given by 6.3 $W^{1/3}$ where W is the weight of LNG in pounds.
2. The LNG vaporizes at a rate (0.037 lbs/ft^2 sec) which is several times higher than would have been predicted.
3. Downwind of the spill, peak concentrations in the vapor trail are as much as 20 times larger than the time-averaged concentrations which are predictable from air pollution equations.
4. Layering of the cold evaporating natural gas has about the same effect on dispersion as a strong temperature inversion in the atmosphere in an air pollution problem.

None of the above conclusions would dictate an adverse decision concerning the transportation of LNG.

Unfortunately, the study raised questions on one aspect of the problem for which no answers are yet available. Small-scale explosions occurred when LNG was poured onto water; no explanation can be offered with confidence for these explosions and no assurance can be offered that these explosions could not scale up to damaging proportions in a massive spill.

It is recommended that further work be carried out with LNG-water. One phase of this work should investigate the details of LNG-water

---

20/ Rinderer, L., and F. Haefer. "Explosive Boiling in Nitrogen Dewars and Nitrogen Shielded Helium Dewars". Cryogenics, September 1962, pp. 288-9.

interaction, particularly to isolate the explosive phenomenon for laboratory study (three candidate mechanisms are postulated in Section V, D). The other phase should comprise massive spill tests to extend the scale of the present program by at least an order of magnitude (the largest instantaneous spill was 480 lbs LNG and the largest steady "leak" rate was 1 lb/sec).

UNCLAS

Security Classification

DOCUMENT CONTROL DATA - R & D

(Security classification of title, body of abstract and indexing annotation must be entered when the overall report is classified)

1. ORIGINATING ACTIVITY (Corporate author)
U.S. DEPARTMENT OF INTERIOR
BUREAU OF MINES

2a. REPORT SECURITY CLASSIFICATION
UNCLASSIFIED

2b. GROUP
6/20, 7/3,

3. REPORT TITLE
HAZARDS OF LNG SPILLAGE IN MARINE TRANSPORTATION

4. DESCRIPTIVE NOTES (Type of report and inclusive dates)
FINAL REPORT - FEBRUARY 1970

5. AUTHOR(S) (First name, middle initial, last name)
BUREAU OF MINES
PITTSBURGH, PENNSYLVANIA
D.S. BURGESS
J.N. MURPHY
M.G. ZABETAKIS

6. REPORT DATE
FEBRUARY 1970

7a. TOTAL NO. OF PAGES
35

7b. NO. OF REFS
20

8a. CONTRACT OR GRANT NO.
MIPR NO. R-700(1)-9-92317

b. PROJECT NO.
79413

c.

d.

9a. ORIGINATOR'S REPORT NUMBER(S)
SRL REPORT NO. S-4105

9b. OTHER REPORT NO(S) (Any other numbers that may be assigned this report)
—

10. DISTRIBUTION STATEMENT
UNLIMITED

11. SUPPLEMENTARY NOTES
NONE

12. SPONSORING MILITARY ACTIVITY
U.S. COAST GUARD

13. ABSTRACT

SEE PAGE 2 OF SUBJECT REPORT.

DD FORM 1 NOV 68 1473

UNCLAS

Security Classification